LUND UNIVERSITY

Differentiation of Central Nervous System Tumors: Multiparametric magnetic resonance imaging with histological, genetic, and prognostic correlations

Durmo, Faris

2021

Document Version:
Publisher's PDF, also known as Version of record

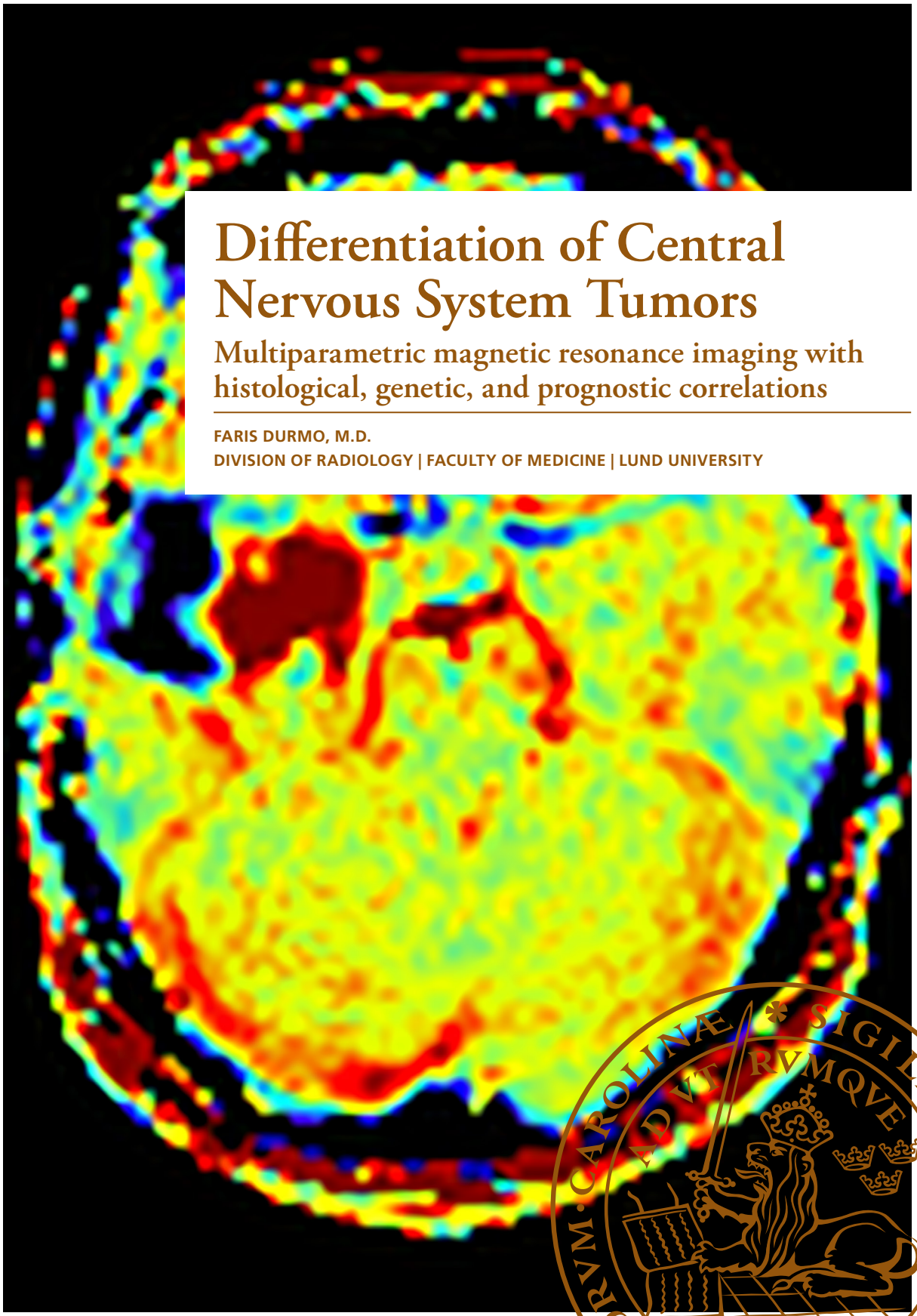

Differentiation of Central Nervous System Tumors

Multiparametric magnetic resonance imaging with histological, genetic, and prognostic correlations

FARIS DURMO, M.D.
DIVISION OF RADIOLOGY | FACULTY OF MEDICINE | LUND UNIVERSITY

Printed by Media-Tryck, Lund 2021 NORDIC SWAN ECOLABEL 3041 0903

Differentiation of Central Nervous System Tumors: Multiparametric magnetic resonance imaging with histological, genetic, and prognostic correlations

Gliomas and metastases comprise most of the neoplasms that are found within the brain. Gliomas, one of the many still remaining historical enemies of medicine and doctors, not just society. Progress has been slow; many have devoted their life to help the medical community and society inch closer to a cure or improvement in clinical outcomes for patients suffering from this devastating disease.

For this thesis, we set out to try and utilize advanced MRI modalities and study brain tumors in adults in the hope of improving upon current level of accuracy in diagnosis, prognosis prediction, histological correlations, and molecular genetic characterization.

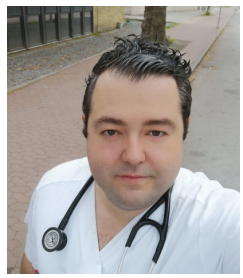

DR. FARIS DURMO M.D. is a father, husband, and a licensed medical doctor; currently employed at the Radiology Department at Lund Univ. and Skåne Univ. Hospital.

LUND UNIVERSITY

FACULTY OF MEDICINE

Department of Clinical Sciences Lund
Division of Radiology

Lund University, Faculty of Medicine
Doctoral Dissertation Series 2021:87
ISBN 978-91-8021-094-2
ISSN 1652-8220

Differentiation of Central Nervous System Tumors: Multiparametric magnetic resonance imaging with histological, genetic, and prognostic correlations.

Differentiation of Central Nervous System Tumors: Multiparametric magnetic resonance imaging with histological, genetic, and prognostic correlations.

Faris Durmo, M.D.
Faculty of Medicine
Division of Radiology, Department of Clinical Sciences
Lund

LUND
UNIVERSITY

DOCTORAL DISSERTATION

by due permission of the Faculty of Medicine, Lund University, Sweden.
To be defended at Lund University; Lecture Hall Segerfalksalen, Sölvegatan 17, 223 62 Lund. 20210922, 13.00-17.00.

Faculty opponent
Professor Dr. Johan Wikström MD., PhD. Department of Surgical Sciences, Radiology and molecular imaging, Uppsala University, Uppsala, Sweden

Organization LUND UNIVERSITY	**Document name** DOCTORAL DISSERTATION
Faculty of Medicine Department of Clinical Sciences Division of Radiology, Lund	**Date of issue** 2021-09-22
Author: Faris Durmo	Sponsoring organization

Title and subtitle Differentiation of Central Nervous System Tumors: Multiparametric magnetic resonance imaging with histological, genetic and prognostic correlations.

Abstract

Background: Gliomas and metastases make up more than 50 % of all brain tumors. The prognosis is poor and survival is short in comparison with other malignant diseases for example prostate cancer or breast cancer, where great strides have been made in the past 20 years in terms of detection and treatments.

Aim: Utilization of advanced MRI modalities for the study of brain tumors in adults for diagnosis, prognosis prediction, histological correlations, and molecular genetic characterization.

Methods: For **paper I**, 3 T MAGNETOM Skyra (Erlangen, Germany) and ADC, FA, CBF, CBV, volumetrics from T1w- and T2w imaging. Imaging biomarkers from perilesional edema, and tumor tissue were analyzed and normalized with contralateral normal appearing white matter. A binary logistic regression model was constructed and evaluated for prediction of LGG/HGG/MET (n = 43). The mean time to progression and overall survival were assessed for the three groups. For **paper II**, ^{1}H-MRS was performed on a 3 T MAGNETOM Skyra (Erlangen, Germany). HGG, MET and LGG patients' brain lesion, edematous tissue, normal appearing white matter tissue in both hemispheres, were retrospectively evaluated for the capability of the metabolic concentrations and their ratios to discern between LGG/HGG/MET (n = 33). Construction of binary logistic regression models from investigated metabolic biomarkers was performed. All significantly differing metabolites and ratios were examined for prognostic capacity in terms of differences in overall survival. For **paper III**, APTw imaging, on a 3 T MAGNETOM Prisma (Siemens, Erlangen Germany) was utilized for prediction of LGG/HGG/MET (n = 26). 2 patients with MET where excluded. A binary logistic regression model was constructed and single and multiple APTw% signals (mean, minimum, max & range) were assessed for discrimination of LGG from HGG. The APTw% signals (mean, max, range) were compared retrospectively with the initial radiological assessment and later prospectively with three radiologists' assessment. For **paper IV**, whole-tumor segmentation of glioblastoma (n = 32) with APTw imaging on a 3 T MAGNETOM Prisma (Siemens Erlangen, Germany) was performed. Subjects were divided into ATRX-mut or ATRX-wt glioblastoma. Mean, Median and maximum APTw% signals were assessed.

Results: In **paper I**, normalized ADC, CBF, CBV in tumor and CBF in edema were significant predictors of LGG/HGG, AUCs = .87, .95,.91, .82. HGG/MET were only differentiable with normalized ADC in edema (AUC = .76, p-value < .015). Normalized ADC, CBF, CBV in tumor, normalized ADC in edema, volume of edema and volume ratio of edema to tumor were significant predictors of LGG/MET, with normalized CBF being the best single biomarker (AUC = .95).

The multivariable logistic regression model (AUCs = 1.00, AUCs .96) outperformed the single biomarkers for differentiation of HGG/LGG and LGG/MET, respectively. In **Paper II**, tLip/tCho (AUC = .905), Ins/tCho (AUC = .905) in lesional tissue (non-enhancing and Gd-enhancing on T1w) were found to be significant predictors of LGG from HGG and MET (AUCs = 1.00, .984, respectively). For HGG/MET, tCr/tCho (AUC = .824) in edematous tissue,

tCho/tCr (AUC = .788), NAA/tCho (AUC = .817) in ipsilateral normal appearing white matter were the sole significant predictors. The multivariable logistic regression model outperformed the single metabolic biomarkers for HGG/LGG (AUC = 1.00) and HGG/MET (AUC = .935) and matched the AUC = 1.00 of tLip/tCho for LGG/MET. In **paper III**, mean, max and range APTw% signals were found to be significant predictors of HGG from LGG (p-values = .005, .002, .033, respectively). The multivariable logistic regression model outperformed any single biomarker in terms of accuracy (AUC = .958) vs. max APTw% (AUC = .948) which was the single best predictor. A generalized cut-off value: mean APTw% > 2.0% showed promise as only 2 cases in the glioma cohort were misclassified. The multivariable model based on mean, max and range APTw% signal misclassified 3 subjects in the glioma cohort (METs excluded). Readers 1 and 2 misclassified 4 subjects each, reader 3 misdiagnosed 7 subjects. In **paper IV**, maximal APTw% signal (cut-off value 3.83%) showed predictive capacity with 100% sensitivity and 69.2% specificity (AUC = .801, p = .023) for ATRX-mut vs. ATRX-wt glioblastoma.

Conclusions: For **Papers I-III**, the multivariable logistic regression model showed either higher or equal accuracy in the binary prediction of HGG/LGG/MET, than single and significant imaging biomarkers. **Paper III** additionally showed the benefit of utilizing APTw imaging in the clinical setting for differentiation of brain tumors and was better compared with radiologists' assessment. **Paper IV** showed for the first time, successful molecular stratification of ATRX-wt from ATRX-mut glioblastoma by MRI and maximal APTw% signal as significant imaging biomarker.

Key words Glioma, Brain Cancer, Tumor, Amide Proton Transfer Imaging, Perfusion, Diffusion, Spectroscopy

Classification system and/or index terms (if any)

Supplementary bibliographical information	**Language** English
ISSN and key title 1652-8220 Lund University, Faculty of Medicine Doctoral Dissertation Series 2021:87	**ISBN** 978-91-8021-094-2

Recipient's notes	**Number of pages 64**	Price
	Security classification	

Signature 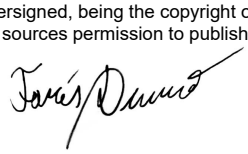 Date 2021-08-01

Differentiation of Central Nervous System Tumors: Multiparametric magnetic resonance imaging with histological, genetic, and prognostic correlations.

Faris Durmo, M.D.

Faculty of Medicine

Division of Radiology, Department of Clinical Sciences

Lund

LUND
UNIVERSITY

Faculty of Medicine
Department of Clinical Sciences, Lund
Division of Radiology

ISBN 978-91-8021-094-2
ISSN 1652-8220

Printed in Sweden by Media-Tryck, Lund University
Lund 2021

To my family, mother, father, sister, wife, son.

My late grandmothers Hanka Durmo and Melća Dedić,
grandfathers Hilmo Durmo and Ahmed Dedić

”Jer vremena ima tako malo
I vremena neće više biti”

-Mehmedalija Mak Dizdar -Kameni Spavac (2004) p. 51

Table of Contents

Abstract **11**

Abbreviations **13**

Populärvetenskaplig sammanfattning **14**

Studies Included in the Thesis **17**

Historical context **18**

The World Health Organization Classification of Tumors of the Central NervousSystem 2016-2021 20
Epidemiology of Glioma 21
Magnetic Resonance Imaging 22
Diffusion Weighted Imaging 23
Diffusion Tensor Imaging 24
Magnetic Resonance 1H-Spectroscopy 25
Perfusion Weighted Imaging 25
Amide Proton Transfer Weighted Imaging 26

Aims **28**

Ethical considerations **29**

Material and Methods **30**

Patients 30
MRI Acquisition protocols 31
Software and segmentation 32
Ethical permissions 34
Statistics 34

Results **36**

Paper I 36
Paper II 37
Paper III 39
Paper IV 42

Discussion **45**
Papers I-II 45
Paper III 49
Paper IV 50
Clinical impact **51**
Future perspectives **52**
Conclusions **53**
Paper I 53
Paper II 53
Paper III 53
Paper IV 53
Acknowledgments **54**
References **55**

Abstract

Title: Differentiation of Central Nervous System Tumors: Multiparametric magnetic resonance imaging with histological, genetic, and prognostic correlations

Background: Gliomas and metastases make up more than 50 % of all brain tumors. The prognosis is poor, and survival is short in comparison with other malignant diseases for example prostate cancer and breast cancer where great strides have been made in the past 20 years in terms of detection and treatments.

Aim: Utilization of advanced MRI modalities for the study of brain tumors in adults for diagnosis, prognosis prediction, histological correlations, and molecular genetic characterization.

Methods: For **paper I**, 3 T MAGNETOM Skyra (Siemens, Erlangen, Germany) and ADC, FA, CBF, CBV, volumetrics from T1w- and T2w imaging. Imaging biomarkers from perilesional edema, and tumor tissue were analyzed and normalized with contralateral normal appearing white matter. A binary logistic regression model was constructed and evaluated for prediction of LGG/HGG/MET (n = 43). The mean time to progression and overall survival were assessed for the three groups.

For **paper II**, ^{1}H-MRS was performed on a 3 T MAGNETOM Skyra (Siemens, Erlangen, Germany) HGG, MET and LGG patients' brain lesion, edematous tissue, normal appearing white matter tissue in both hemispheres, were retrospectively evaluated for the capability of the metabolic concentrations and their ratios to discern between LGG/HGG/MET (n = 33). Construction of binary logistic regression models from investigated metabolic biomarkers was performed. All significantly differing metabolites and ratios were examined for prognostic capacity in terms of differences in overall survival.

For **paper III**, APTw imaging, on a 3 T MAGNETOM Prisma (Siemens, Erlangen Germany) was utilized for prediction of LGG/HGG/MET (n = 26). MET later excluded due to (n = 2). A binary logistic regression model was constructed and single and multiple APTw% signals (mean, minimum, max & range) were assessed for discrimination of LGG from HGG. The APTw% signals (mean, max, range) were compared retrospectively to the initial radiological assessment and, later, prospectively with three radiologists' assessment.

For **paper IV**, whole-tumor segmentation of glioblastoma (n = 32) with APTw imaging on a 3 T MAGNETOM Prisma (Siemens Erlangen, Germany) was performed. Subjects were divided into ATRX-mut or ATRX-wt glioblastoma. Mean, median and maximum APTw% signals were assessed.

Results: In **paper I**, normalized ADC, CBF, CBV in tumor and CBF in edema were significant predictors of LGG/HGG, AUCs = .87, .95,.91, .82. HGG/MET were only differentiable with normalized ADC in edema (AUC = .76, p-value < .015). Normalized ADC, CBF, CBV in tumor, normalized ADC in edema, volume of edema and volume ratio of edema to tumor were significant predictors of LGG/MET, with normalized CBF being the best single biomarker (AUC = .95). The multivariable logistic regression model (AUCs = 1.00, AUCs .96) outperformed the single biomarkers for differentiation of HGG/LGG and LGG/MET, respectively. In **Paper II**, tLip/tCho (AUC = .905), Ins/tCho (AUC = .905) in lesional tissue (non-enhancing and Gd-enhancing on T1w) were found to be significant predictors of LGG from HGG and MET (AUCs = 1.00, .984, respectively). For HGG/MET, tCr/tCho (AUC = .824) in edematous tissue, tCho/tCr (AUC = .788), NAA/tCho (AUC = .817) in ipsilateral normal appearing white matter were the sole significant predictors. The multivariable logistic regression model outperformed the single metabolic biomarkers for HGG/LGG (AUC = 1.00) and HGG/MET (AUC = .935) and matched the AUC = 1.00 of tLip/tCho for LGG/MET. In **paper III**, mean, max and range APTw% signals were found to be significant predictors of HGG from LGG (p-values = .005, .002, .033, respectively). The multivariable logistic regression model outperformed any single biomarker in terms of accuracy (AUC = .958) vs. max APTw% (AUC = .948) which was the single best predictor. A generalized cut-off value: mean APTw% > 2.0% showed promise as only 2 cases in the glioma cohort were misclassified. The multivariable model based on mean, max and range APTw% signal misclassified 3 subjects in the glioma cohort (METs excluded). Readers 1 and 2 misclassified 4 subjects each, reader 3 misdiagnosed 7 subjects. In **paper IV**, maximal APTw% signal (cut-off value 3.83%) showed predictive capacity with 100% sensitivity and 69.2% specificity (AUC = .801, p = .023) for ATRX-mut vs. ATRX-wt glioblastoma.

Conclusions: For **Papers I-III**, the multivariable logistic regression model showed either higher or equal accuracy in the binary prediction of HGG/LGG/MET, compared with single and significant imaging biomarkers. **Paper III** additionally showed the benefit and advantage of utilizing APTw imaging in the clinical setting for differentiation of brain tumors compared to only radiologists' assessment of standard MR sequences. **Paper IV** showed for the first time, successful molecular stratification of ATRX-wt from ATRX-mut glioblastoma by MRI and maximal APTw% signal as significant imaging biomarker.

Abbreviations

GBM – Glioblastoma Multiforme
GB – Glioblastoma
HGG – High Grade Glioma
LGG – Low Grade Glioma
ATRX – Alpha-thalassemia/mental retardation, X-linked
IDH – Isocitrate dehydrogenase
1p19q codeletion – Short arm and long arm of chromosomes 1 and 19 deletions
P53 – Protein 53
Ki-67 index – mitotic index using the nuclear protein ki67
MGMT - DNA repair enzyme O^6-methylguanine-DNA methyltransferase
MRI – Magnetic Resonance Imaging
MRS – Magnetic Resonance Spectroscopy
MRSI - Magnetic resonance spectroscopy imaging
FA – Fractional anisotropy
CBF – Cerebral blood flow
CBV – Cerebral blood volume
MTT – Mean Transit Time
ADC – Apparent diffusion coefficient
DWI – Diffusion Weighted imaging
DSC – Dynamic susceptibility contrast MR perfusion
DCE – Dynamic contrast enhanced MR perfusion
DTI – Diffusion tensor imaging
DKI – Diffusion kurtosis imaging
PWI – Perfusion weighted imaging
APTw – Amide proton transfer
TR – Repetition time
TE – Echo time
IR – Inversion recovery
STIR – Short tau inversion recovery
FLAIR – Fluid-attenuated inversion recovery
T1w – T1weighted imaging
T2w –T2weighted imaging
TSE – Turbo spin echo
GRE – Gradient echo
WHO – World Health Organization

Populärvetenskaplig sammanfattning

Cancer som spridit sig till hjärnan och primära hjärntumörer av typen gliom, utgör mer än hälften av alla hjärntumörer. Avhandlingens fokus har varit gliomatösa hjärntumörer men även cancer som uppstått i andra organ och spridit sig till hjärnan. I dagsläget används kirurgi, strålningsterapi och cytostatika som de främsta medlen för att bekämpa dessa tumörer. Avseende uppkomsten och riskökning för gliom i hjärnan är inte mycket känt. Olika former av skadlig strålning mot hjärnan, alkohol och upprepade skallskador har förts fram som möjliga orsaker till ökad risk för utveckling av hjärntumör. Med ny teknik som datortomografi och magnetkamera-undersökning har nya möjligheter öppnats upp för diagnostik, behandlingsplanering och även kirurgiskt stöd i form av 3D-modellering och intraoperativ magnetkamera-undersökning. Avancerad magnetresonanstomografi, MRT, har utvecklats i rask takt de senaste 20 åren och idag kan man avbilda inte bara tumören men även cerebralt blodflöde, blodvolym, koncentrationer av hjärnans olika molekyler, lipider, och proteiner. Utöver detta kan man också avbilda hjärnan med tekniker som använder sig av vattenmolekylers rörelser i olika medier, så kallad diffusionsviktad MRT. En något nyare teknik är amidproton-transfer magnetresonanstomografi, APT MRT, Det är en teknik som utnyttjar fria protoner i amidgrupperna på proteiner. Genom att tillföra energi i form av radiovågor, kan man påtvinga dessa protoner att de antingen byter plats med protonerna i vattenmolekylerna eller att de avger sin överskottsenergi till protonerna i vattenmolekylerna. Det som man erhåller då är en signalskillnad i den totala vattensignalen; denna skillnad medför att man kan skapa en kontrast mellan vävnader och därmed avbilda tumörer och andra strukturer.

Denna avhandling består av fyra studier, varav tre är publicerade och den sista är i manuskript-format. Målet har varit att via avancerade MR tekniker utforska radiologiska biomarkörer för diagnostisk nytta, prognostisering av sjukdom, överlevnadsanalys, histologiska och patologiska överensstämmelser mellan uppmätta och kvantifierade biomarkörer samt potentiellt tillämpa bildtekniker för att matcha avvikelser i biomarkörer med förlust av gen-uttryck.

Studie I, visade att kombinationen av olika MRT sekvenser såsom diffusion och perfusion tillsammans med volymmätningar, i och av olika delar av tumören i hjärna på ett mer säkert sätt diagnosticera och urskilja hjärntumörer från varandra. Via en

algoritm för prediktion av två möjliga utfall, kunde de biomarkörer vars kvantitet vi fastställt sättas in i algoritmen som ytterligare information. Denna information visades sedan kunna urskilja metastaser från låggradigt maligna och höggradigt maligna hjärntumörer av typen gliom. Detta genom att mäta vattenmolekylers slumpmässiga förmåga att röra sig i en riktning obehindrat/delvis hindrat i ett objekt av en viss densitet (s.k. diffusion och fraktionell anisotropi), mängden blodflöde och blodvolym (perfusion), volymen av tumör, ödem, ratio av ödem- och tumörvolym, kunde man kombinera värdena från dessa i en matematisk modell som ökade träffsäkerheten i diagnosticerandet av låggradiga – och höggradiga gliom och särskiljandet av gliom från metastaser.

I studie II, tillämpades en teknik ^{1}H-MRS (MR spektroskopi) där icke normal vävnad i och runt tumör undersöktes genom att mäta biokemiska förändringar i hjärnan. Koncentrationer av metaboliter som kreatin, fetter, och aminosyror uppmättes i olika delar av hjärnan och i tumören såsom: frisk vit substans i samma hemisfär som tumören är lokaliserad samt i kontralateral hemisfärs friska vita substans, cystisk komponent eller misstänkt vävnadsdöd i tumör s.k. nekros, icke- och kontrastuppladdande tumörvävnad samt ödem. Kvoten lipider och kolin samt inositol och kolin uppmätta i icke- och kontrastuppladdande tumörvävnad visade sig vara bäst på att särskilja mellan låggradiga och höggradiga gliom och metastaser. Särskiljandet av höggradiga gliom från metastaser kunde påvisas av kvoten kreatin/kolin i ödem samt kvoterna kolin/kreatin och N-acetylaspartat/kolin i normal vit substans i samma hjärnhemisfär relativt till tumörlokalisation. Även i denna studie tillämpades en matematisk modell som tillät kombinerandet av information från alla uppmätta biokemiska förändringar i hjärnan, s.k. biomarkörer. I jämförelse med enskilda biomarkörer, visade modellen sig ha en lika bra eller bättre träffsäkerhet i urskiljandet av låggradiga gliom och höggradiga gliom från varandra och metastaser.

I **studie III**, undersöktes värdet av MRT APT genom måttet på maximal, minimum, medel och intervall av APTw% signalen i områden med observerad maximal avvikelse i signal. Maximal, medel och intervall visade sig kunna särskilja mellan låggradiga och höggradiga gliom. Genom att inkorporera dessa biomarkörer i en matematisk modell, kunde träffsäkerheten öka i diagnostiskt urskiljande av dessa tumörtyper. Modellen och biomarkörerna jämfördes med den första radiologiska klassificeringen på sjukhuset genom etablerandet av gränsvärden för biomarkörerna. Därefter jämfördes tre radiologers diagnostiska bedömning med modell och enskilda biomarkörers träffsäkerhet. Biomarkörerna visade sig vara ett viktigt komplement till den kliniska radiologiska bedömningen av hjärntumörer. I **studie IV**, undersöktes om MRT APT kunde urskilja mellan glioblastom som förlorat uttryck av ATRX och de glioblastom som hade bevarat uttryck. Här visar vi att MRT-APT kan särskilja dessa olika typer av gliom baserat på deras maximala APTw% signal, där gränsvärde för 3,83% hade bäst avvägd prediktiv kapacitet med 100% sensitivitet och 69,2% specificitet.

Studies Included in the Thesis

I. **Durmo, F**., Lätt, J., Rydelius, A., Engelholm, S., Kinhult, S., Askaner, K., Englund, E., Bengzon, J., Nilsson, M., Björkman-Burtscher, I. M., Chenevert, T., Knutsson, L., & Sundgren, P. C. (2018). *Brain Tumor Characterization Using Multibiometric Evaluation of MRI*. Tomography: A Journal for Imaging Research, 4(1), 14–25. https://doi-org.ludwig.lub.lu.se/10.18383/j.tom.2017.00020

II. **Durmo, F**., Rydelius, A., Baena, S. C., Askaner, K., Lätt, J., Bengzon, J., Englund, E., Chenevert, T. L., Björkman-Burtscher, I. M., & Sundgren, P. C. (2018). *Multivoxel ^{1}H-MR Spectroscopy Biometrics for Preoperative Differentiation Between Brain Tumors*. TOMOGRAPHY, 4(4), 172–181. https://doiorg.ludwig.lub.lu.se/10.18383/j.tom.2018.00051

III. **Durmo, F**., Rydhög, A., Testud, F., Lätt, J., Schmitt, B., Rydelius, A., Englund, E., Bengzon, J., van Zijl, P., Knutsson, L., & Sundgren, P. C. (2020). *Assessment of Amide proton transfer weighted (APTw) MRI for pre-surgical prediction of final diagnosis in gliomas*. PLoS ONE, 15(12), 1–25. https://doiorg.ludwig.lub.lu.se/10.1371/journal.pone.0244003

IV. **Durmo, F**., Lätt, J., Rydelius, A., Englund, E., Bengzon, J., van Zijl, P., Knutsson, L., & Sundgren, P. C. *Amide proton transfer weighted (APTw) MRI predicts ATRX expression status in glioblastoma*. Unpublished Manuscript

Historical context

The first documented case of simultaneous utilization of anesthesia, antiseptic routines and cerebral localization of a tumor concomitantly with a neurosurgical intracranial procedure is dated back to 1879 in Glasgow[1]. The first documented modern operation on a patient with a glioma tumor was performed by R Godlee on November 25, 1884[2]. Patients with tumors of the skull and meninges had, before 1879, undergone attempts by physicians to be treated surgically. However, they were only done so on patients with easily identifiable outgrowths either pushing or going through the cranium[3]. Dr William W. Keen, professor of the principles of Surgery and of Clinical Surgery at Jefferson Medical College, was one of those who recognized the challenges with diagnosing brain tumors. By the end of the 19th century, neurosurgeons relied heavily on the ophthalmologists and neurologists for establishing the correct diagnosis and location of the brain tumors. Excerpts as follows from page 1 in[4]: "The chief difficulty in the surgical treatment of intracranial tumors is unquestionably the lack as yet of means of making an absolutely exact diagnosis of the location, size, and number of such tumors. (…) Possibly the recent discovery of Röntgen may assist us. By this he has achieved what has heretofore been regarded as impossible, — namely, by means of the cathodic rays from Crookes's tubes of skiagraphing" internal parts of the body. Whether intracranial tumors will be also as permeable to these rays as are other soft parts of the body we do not yet know. (…) Until this discovery is further developed and made actually available, we must rely on the existing methods of cerebral localization."

Godlee[2], utilized the brain topography as suggested by Ferrier[5,6] tying neuroanatomy to function. Bennett and Godlee[2] deduced that the cortex, near the middle part of the Rolandic fissure on the right side (sulcus centralis dx) ought to be involved due to motor phenomena present in the patient, no sensation deficits, paroxysmal seizures. Patient exhibited complete paralysis of hand and fingers, loss of supination and pronation of the forearm, partial paresis at the level of the elbow and partial paresis at the level of shoulder joint apart from minor paresis of leg and face[2]. Apart from this the patient presented with bilateral optic neuritis, a slight paresis of left side of the face when impressed to force a movement, no sensory deficits of the face, tongue deviated slightly to the left, no dysarthria present[2]. This, careful assessment of symptoms without external tell signs, enabled them to identify that the lesion was probably located in the post central gyrus and also encompassed parts of the frontal gyrus[2]. Upon rotation of the head to the left, patient experienced paresthesia in the

form of a "peculiar feeling" running down left side of the neck, onto the arm and leg with patient soon after losing consciousness and going into a generalized seizure[3]. Of note, the generalized seizures stopped recurring after the upper extremities began to exhibit progressive weakness[3]. Dr Bennett, made the call where the lesion was located, but Kirkpatrick argues that this was probably done after discussions with neuroanatomists and neurologists[3]. Given the team-effort in localizing the lesion, and the deciphering of symptomatology across several months, it is not surprising there were debates as to where and how tumors arose in the brain.

Bramwell[7] reported on other discrepancies noted in patients and presentation. For example, in some a great increase in intracranial pressure and in others little or none with scant irritation of the cerebrum[7]. At the time there was also a disagreement in the location of preference for the glioma within the brain[7]. Byrom Bramwell proposed zones within the white matter where gliomas were of preference and more frequent before it spreads to cortex and causes irritation with symptomatology. This was in contrast to another contemporary prominent researcher at the time such as Ziegler who proposed that the glioma started out in close proximity to the pia mater[7].

Historically the glioma was identified as occurring in any part of the brain, varying in size and a common propensity to infiltrate large volumes of the brain[7]. Structurally, an important finding even in the 19th century was the extensive vascularity found in glioma tumors, i.e. large vessels with thin walls[7].

There was no distinction between different types of tumors at the late 19th century, varied growth with very rapid infiltration in some cases and in others where the tumor has been present for multiple years[7]. Berns in 1800 and Abernety in 1804, described the first non-metastatic primary brain tumor[8]. They were merely grossly described and defined as diffuse tumors as they had no distinct border with seemingly healthy brain tissue[8]. In the first half of the 19th century, the primary brain tumors of presumable glial origin had different names; medullary sarcoma (in British literature), fungus medullare (in German literature) and encéphaloïde (in French literature)[8]. Previous to Godlee and Bennett's work[2], gliomas were obtained from post mortem subjects via autopsy studies[9]. The collection of material for microscopy was therefore limited to available post mortem subjects[9]. Despite this, Rudolf Virchow managed to perform the first systematic histological description of glial tumor morphology in 1865[8]. Virchow identified the glial cells as origin for the malignant tumors and gave them the name glioma[8,10]. Based on histological discrepancy in cellularity and appearance in pathological tissue versus normal tissue, he stratified the malignancies into two distinct groups; low grade glioma (LGG) and high grade glioma (HGG)[8,10]. Virchow's classification of glioma corresponds to the WHO classification of 2016, with LGG being comprised of WHO grade 1-2 and HGG being WHO grades 3-4[8,10,11]. With Wilhelm Röntgen and the discovery of Roentgen rays we now know as x-rays in 1895[12] a technique was formed that could help in the now century long endeavors in diagnosing, locating and operating on patients with brain tumors. Neurosurgeon Cushing found

applications for tumors near sella turcica, while Fedor Krause incorporated the technique in clinical routine for localization of brain tumors[12]. 1904 the first article on x-rays utility on brain tumors and infarctions was published in the Transactions of the American Roentgen Ray Society[12]. Dr Cushing's neurosurgeon colleague at Johns Hopkins University; Dr Dandy was the first to identify the possible utility of air and x-rays in combination[13] for visualization of the brain i.e. pneumoencephalography, for which he was awarded with the Nobel Prize in 1933[12]. It is somewhat peculiar then that Dr Cushing touted the new technique as limited in the diagnosis of brain tumors as it helped forward the entire field of neurosurgery and opened up a new field; neuroimaging[12]. Another landmark paper[14], published in 1924 reported the utilization of air ventriculograms in 532 patients[12,14]. Small supratentorial or infratentorial masses were difficult to visualize but more than adequate for sufficiently sized supratentorial masses[12,14]. The direct access to resected tumors, after Godlee's safe removal of a brain tumor in 1884[2], and other advancements in neurosurgery in the late 19th century, opened up new possibilities for systematic histopathological classification and characterization of brain tumors[9]. In 1926 Percival Bailey and Harvey Cushing published the first classification of brain tumors since Virchow[8], where they named the most histologically atypical and clinically most malignant tumor entity – Spongioblastoma Multiforme, which were later replaced with glioblastoma multiforme GBM[8,15]. Scherer followed up on the classifications of Bailey and Cushing and introduced a whole-tumor approach for diagnosis[8]. The small sample and individual tumor cells previously being referenced as sufficient for diagnosis was deemed non-adequate as for example some glioblastoma multiforme exhibited high diversity in their biological behavior[8]. Subsequently, Scherer introduced the terms primary GBM and secondary GBM[8,16]. The primary entity was the most aggressive entity and had the lowest survival, while the secondary GBM had a less malignant course with reduced progression and increased survival time relative to the primary GBM[8,11,16].

The World Health Organization Classification of Tumors of the Central NervousSystem 2016-2021

Apart from the introduction of new tumor- and subtypes, the biologic and molecular entity of tumors have been better defined and their natural histories have been more optimally characterized when comparing the classification from 2016[11] with the one from 2021[17,18]. Improved understanding of prognosis, improved homogenization of patients for inclusions in clinical trials and also enable choosing a more optimal therapy for patients with particular brain tumors[17]. As this thesis and its studies overlapped with the 2016 WHO classification, the 2021 classification has not been utilized.

Epidemiology of Glioma

It has been established the most frequently occurring, primary malignant intracranial tumor in adults is of glial origin, i.e. glioma[19]. Majority are malignant but some may exhibit intermittent propensities in behavior which may not define them entirely as malignant[19]. The glioma incidence vary across, age at diagnosis, gender, country, race and histologic typing with incidence rates heavily dependent on data collection modus operandi[19]. Proposed incidence across 100k population ranges from 4.67 to 5.73 for all types of glioma while glioblastoma ranges from 0.59 to 3.69 in 100k[19]. Both glioblastoma WHO grade IV and anaplastic astrocytoma grade III increase in frequency with increasing age and peak in the age range 75-84[19]. The sex differences manifest as higher incidence in males vs. females for glioma in general, while non-Hispanic Caucasians have a higher incidence reported than African Americans, Asians/Pacific Islanders or American natives[19].

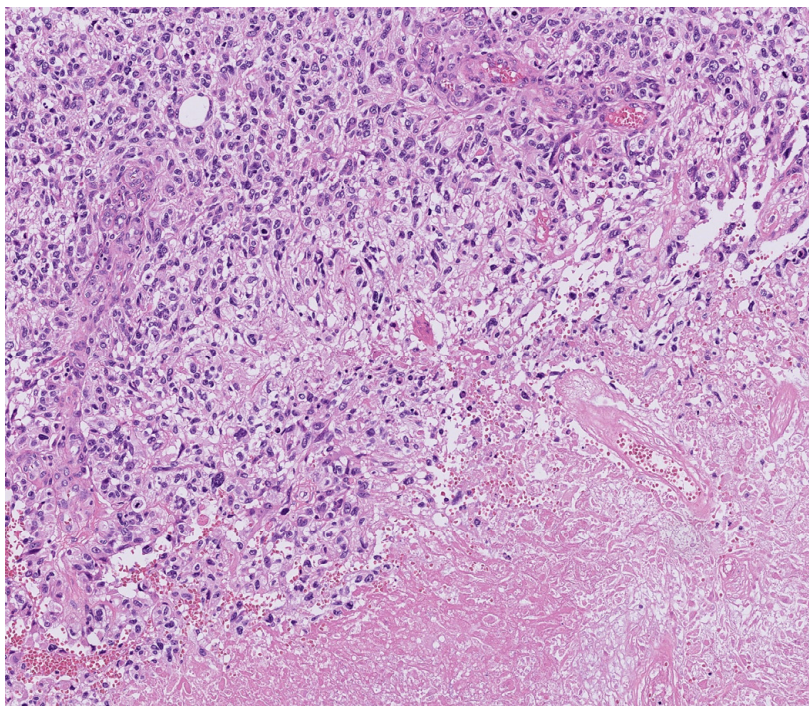

Figure 1.
Glioblastoma Hematoxylin and Eosin stain. Reproduced by permission from Dr Elisabet Englund, Department of Clinical Sciences/Division of Pathology, Lund University, Lund, Sweden. Poorly differentiated and pleomorphic cells. Widespread nuclear atypia with increased mitotic activity, large necrotic area.

Magnetic Resonance Imaging

Prior to the arteriography developed by Moniz in 1927 and the adaptations of Dandy on pneumoencephalography in 1918 there was a high emphasis on neurological examinations and symptomatology for tumor localization[9]. The combination of these two techniques allowed for the first preoperative visualization of masses in the brain[9]. These techniques were later superseded by CT, computed tomography, developed by Cormack and Hounsfield[20,21]. After the advent of CT[22], magnetic resonance imaging (MRI) was brought forward by Lauterbur and Mansfield[9]. Studies comparing MRI with CT showed MRI superior to CT in diagnostic performance when it came to demyelinating disease[23], imaging of structures in the posterior fossa[24], detection and characterization of structural abnormalities in the brain[25]; 16 out of 26 patients not showing pathology on CT, was detected with MRI[26] albeit early comparisons with CT and non-contrast enhanced MRI showed no clear advantages with MRI over CT[27].

Clinical applications have taken a leap over the past 30 years in the MRI field[28] with different MRI sequences being used in distinction, grading of brain lesions but also identifying molecular subtypes, surgical planning and identifying malignant transformation and treatment effects that may mimic those of viable tumor[28]. The conventional MRI with Gd-enhancement has demonstrated to not be optimal for stratification of glioma across grades nor differentiation from other type of lesions[28,29]. The appearance of glioblastoma on T1w contrast enhanced imaging may not be optimal for histopathological correlations, cell density may be increased in both non-enhancing and enhancing parts of tissue[30,31].

The technical background to MRI is that the MR scanner, after installation, itself produces a strong magnetic field which is 30-60 000 times stronger than the Earth's magnetic field, depending on field strength 1.5-3 T. This field is defined as B_0[32]. The MRI system utilizes the inherent nuclear spin and the magnetic properties inherited by proxy of the aforementioned[32]. M_0 is per definition the net equilibrium magnetization vector and increases when B_0 increases[32]. Because of the fixed locations of protons relative to B_0, now the vector M_0 rotates with a known frequency called the Larmor frequency $\omega 0 = \gamma B_0$. γ is the gyromagnetic ratio, a fixed constant for all protons. Upon adding coils or loops of wire, a time varying magnetic field is created and a current induced[32]. This current is induced when M_0 is diverted from its equilibrium orientation (from z-axis to transverse x-y plane)[32]. This is achieved with radiofrequency pulses of a given amplitude and time duration, where a 90° pulse will flip the magnetization vector from z-axis to the transverse plane, note that a 180° flips M_0 from +z to -z[32]. T1 relaxation represents the magnetization recovery back to M_0, while T2 relaxation represents the magnetization going towards zero. Different tissues have different and fixed T1 and T2 relaxation which enables a theoretical separation of these tissues[32]. Echo time (TE), and repetition time (TR) are used for changing the image contrast[32]. TE adjustment in terms of

duration controls the level of T2-weighted contrast being collected as a signal for image acquisition[32]. While T1-weighted contrast is dependent on the level of TR. IR or inversion recovery can be used to suppress signal from a tissue; in fluid-attenuated inversion recovery (FLAIR) it is water and in short tau inversion recovery (STIR) it is fat[32]. This is performed by adding a 180° RF pulse and matching the timing of added pulse to that of longitudinal relaxation of the given tissue one wants to exclude obtaining a signal from[32]. Frequency encoding and phase encoding are used during the collection of signal and used for creating a two-dimensional image by Fourier transformation[32].

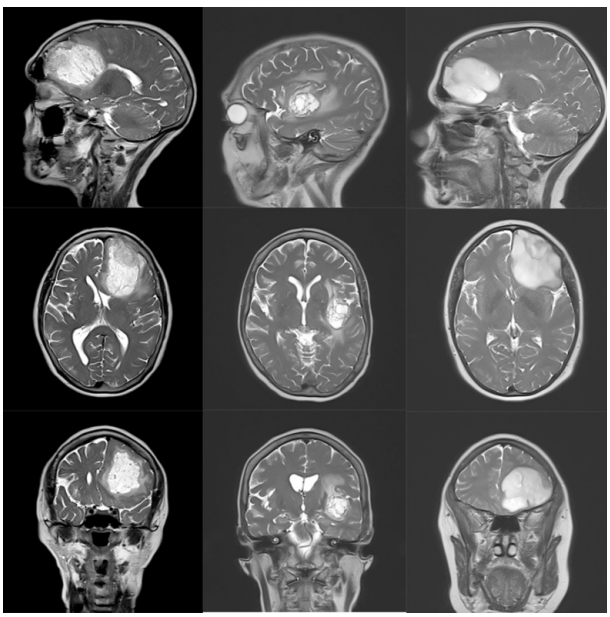

Figure 2.
T2Haste, three patients; left showing high grade glioma, middle metastasis and right a low grade glioma.

Diffusion Weighted Imaging

Free water protons' in tissue mean distanced travelled for the duration of a pulse sequence (owing to Brownian motion) is the contrast produced by diffusion weighted imaging (DWI)[32–35]. Brownian motion is by definition the random movements of microscopic particles as a consequence of collisions by molecules in that same medium[36–38]. ADC, Apparent diffusion coefficient (ADC) is a parameter which is measured in mm^2/s[32,35,39,40]. If extracellular space is rendered into a fluid without any diffusion restriction, the Brownian motion – governed diffusion reaches distances around 10 micrometers[32,40]. Intracellular space is filled with organelles, dynamic environment with membranes and vesicle transport which impact the

diffusion and thus renders the diffusion length less than that of extracellular space[32,33]. The measured ADC, can then by proxy be said to be determined by the influences of ratio water within a cell or entity with a cell membrane[32] and showed by Moseley et al. that diffusion signal intensities in cat nervous system depend on fiber orientation[41]. Necrosis and edema of vasogenic type reduce the net cellularity in tissue, making DWI suitable for differentiation of tumors with high cellularity (HGG, MET for example) from those of lesser cellularity (LGG)[32,42–46].

Diffusion Tensor Imaging

DTI is a modification of DWI, enabling the acquisition of at least 6 directions. The so called 3D-tensor, is a three dimensional vector matrix and approximation of both magnitude and direction of the water diffusion for each obtained voxel[32,40,47]. The increased number of directions in comparison with ADC, yields a more accurate approximation of the direction of water diffusion[32]. The level of anisotropy is defined as, the amount of faster diffusion in one direction vs. one other direction in one voxel[32,48,49]. Fractional Anisotropy (FA) is a scalar measure which can quantify the degree of anisotropy and has been used for approximation of the architecture of microstructures; white matter tracts[32,47–49]. DTI as an advanced MRI technique can assess microinvasions of white matter tracts by for example higher grades of glioma; anaplastic astrocytoma and glioblastoma[32]. In doing so, radiation necrosis, edema, tumor recurrence, and gliosis can be differentiated by DTI[32,50–54]. There has been some mixed success in the definition of margins in white matter tracts presumed infiltrated by glioma, similarly also for the differentiation of vasogenic edema and tumor infiltration[32,52,55–61].

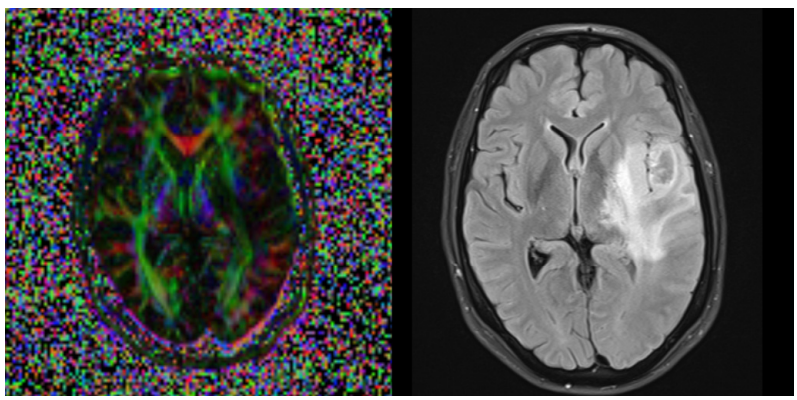

Figure 3.
High Grade Glioma, left fractional anisotropy FA, right accompanying FLAIR sequence.

Magnetic Resonance 1H-Spectroscopy

MRS was developed in the 1980s and initial attempts on patients were spectroscopy utilizing 31phosphorus[62,63] , later ^{1}H-spectroscopy was developed by use of the PRESS-sequence (Point-RESolved spin echo)[28] and thus the hydrogen, ^{1}H- NMR chemical shift spectra could be used for in-vivo observations of metabolites[64]. The PRESS sequence has previously been compared to the STEAM sequence[63], while the STEAM sequence uses three 90° RF pulses, the PRESS utilizes one 90° and two 180° RF pulses and gets twice the signal vs. the STEAM[63]. Of note is also that single voxel MRS is faster and can be deployed somewhat easier than multivoxel MRS (MRSI)[63]. The MRSI has the advantage of being able to measure metabolites at several voxel of interest VOI sites[63].

Several metabolites are available via 1H-MRS such as N-acetylaspartate, Choline, Creatine, Lactate, myo-Inositol, Glutamate/Glutamine[63]. High levels of Choline have been reported in[63] and implicated in glial cells[65], demyelination[66], inflammation[67]. Lactate increases have been shown to occur in hypoxic settings[63,68], in the presence of ischemic brain injury[69,70] and also in brain tumors [71] and in non-glial brain tumors[72].

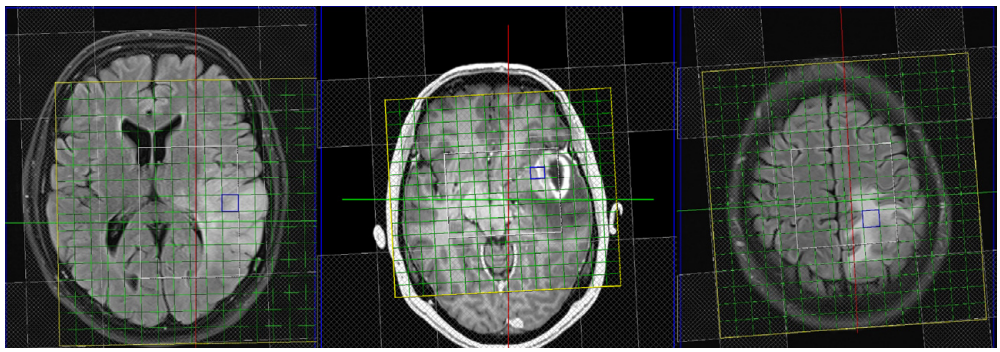

Figure 4.
Multivoxel spectroscopy of left, FLAIR and low grade glioma, middle high grade glioma T1w Gd enhanced, right FLAIR of metastasis.

Perfusion Weighted Imaging

PWI, perfusion weighted imaging techniques[73–75]; blood flow (F) is measured in ml min^{-1} / 100 g tissue within the capillary mesh or network, blood volume (V) mL per 100 g, mean transit time MTT (s) time for passage from capillary to venous side and related physiologically[76] as proposed by Meier and Zierler[77] as F= V / MTT. (DSC) Dynamic susceptibility contrast T1-weighted MRI was shown, in the setting of stroke, to be able to quantify the perfusion within grey and white matter in the brain, verified by previous methods by positron emission tomography PET[78]. Another method that can be utilized for imaging and probing the microcirculation is DCE

(Dynamic Contrast-enhanced) MRI[79], furthermore it can be used to explore the angiogenesis aspect of tumors[79,80]. Perfusion techniques have also been shown to be able to discern low grade gliomas from high grade gliomas[81].

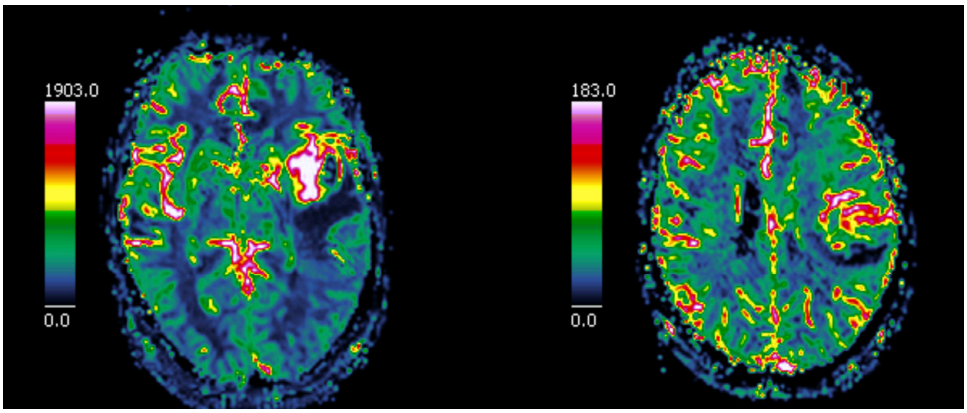

Figure 5.
PWI of a glioblastoma, left Cerebral Blood Flow and on the right Cerebral Blood volume.

Amide Proton Transfer Weighted Imaging

Forsen and Hoffman[82] showed rapid chemical exchange reactions could be probed and studied by NMR techniques[31,82]. At the time Balaban and co-authors[83] showed and proposed chemical exchange sites for utilization as CEST (chemical exchange dependent saturation transfer), metabolites could be imaged based on water proton exchange rates with the help of saturation transfer techniques[83]. They proposed 5-hydroxytryptophan as a CEST contrast agent[83]. Several other biomolecules have been proposed as possible CEST agents[31,84–88]. By utilization of the amide protons in mobile proteins[89,90], a signal can be obtained[31,91]. Amide proton transfer weighted imaging has been applied to assessment of brain tumor burden[31,92], correlated with increased protein concentration in malignant tumors[93–95], identification of genetic markers in gliomas[96,97] and is one of the most widely utilized CEST-techniques[31].

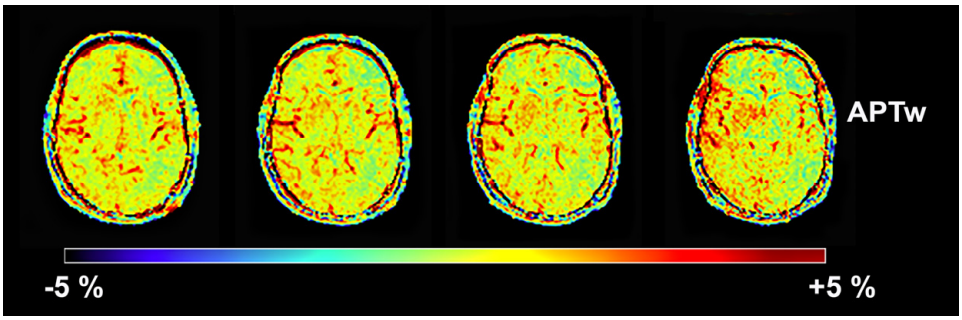

Figure 6.
APTw imaging of a high grade glioma showing increased APTw% signal in right hemisphere, putamen and globus pallidus mostly engaged.

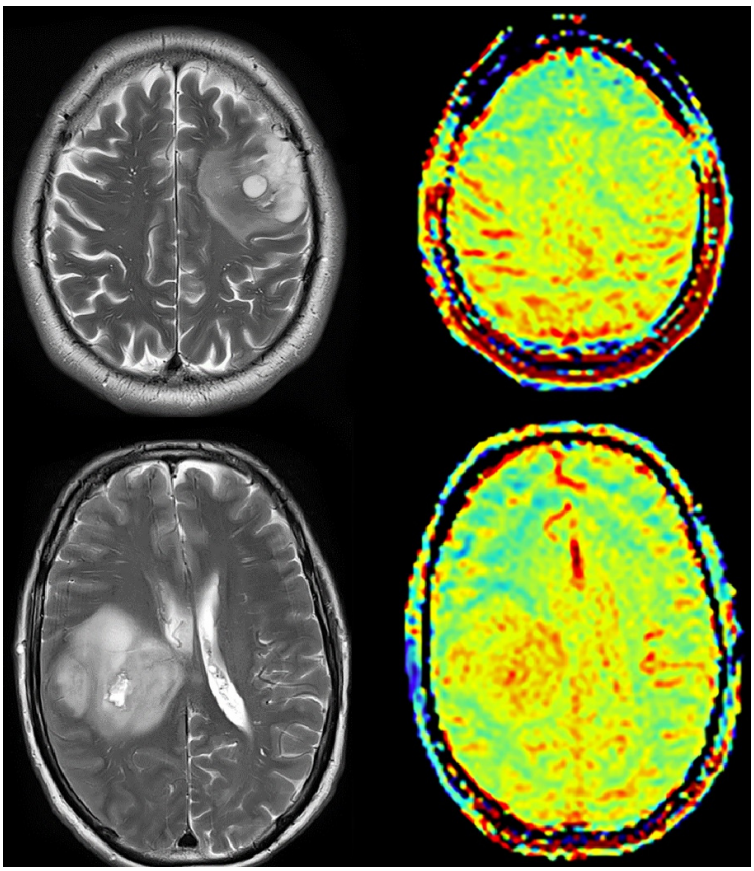

Figure 7.
T2Haste and APTw imaging of a high grade glioma bottom showing increased APTw% signal in right hemisphere, and top low grade glioma with scant increase in APTw% signal.

Aims

The permeating objective of this thesis was to utilize conventional MRI techniques concomitantly with more novel techniques such as Amide Proton Transfer Imaging to improve and investigate ways of diagnosing brain tumors in adult patients.

The paper specific aims are as listed:

I. The aim of this study was to evaluate the sensitivity and specificity of advanced magnetic resonance (MR) imaging metrics for DWI, perfusion-weighted MRI and tumor and edema volume for tumor type differentiation in a cohort of patients with HGG, LGG, and MET.

II. The aim of this study was to use a machine learning algorithm and combine significantly different metabolic data, from healthy-appearing regions and tumor regions in patients with LGG/HGG/MET to increase diagnostic accuracy for preoperative differentiation and prognosis of patients with MET, LGG, and HGG.

III. The primary aim of this study was to evaluate if noninvasive APTw MRI can, in daily clinical routine, increase the radiological accuracy in differentiating less malignant tumors from more malignant ones, i.e., LGG from HGG, prior to surgery. The second objective was to examine if discrepancies between radiological diagnosis and histopathological diagnosis occur to the same degree as previously reported in the literature.

IV. The aim was to assess the ability of APTw MR imaging capabilities to differentiate glioblastoma in terms of ATRX (alpha-thalassemia/mental retardation, X-linked) expression: ATRX wildtype (ATRX-wt) versus loss of ATRX (ATRX-mut).

Ethical considerations

Brain tumors affect both sexes, in this study both men and women were included. Epidemiologically, males are slightly overrepresented in terms of tumor incidence. Even though the slight increase in incidence, the studies have been skewed towards males. This can have multiple reasons. One might be more females opting out of being part of the studies due to increased scan time or fears of impact on quality of life. Other issues might be the timing or setting where the question of study inclusion is posed. Being handed a tumor diagnosis is a life-changing event and devastating occurrence both for patients, families and relatives and wrought with heavy feelings of anxiety and emotional pain. Being asked to participate in a study without any guarantee of benefit, the participating patients did not gain any direct benefits from the results of individual studies as no change in clinical practice or treatment occurred during the time of the studies. Patients need time to process the new diagnosis and all it entails. Therefore, when including, there is a high need to be flexible and adapted to the individual and its needs. The patients are informed that the results from these studies might change future practice, diagnosis and treatment and help future brain tumor patients. One future aspect would be to gain permission to interview those that opted out of the studies or their partners to see if the inclusion process might be improved in any way.

There are safety aspects of MRI which impact choice of modality and usage of Gd intravenous administration. The conventional MRI modalities have the shortcomings that they are minimally invasive and dependent on Gadolinium to enhance contrast-effects. Gadolinium contrast media can among other adverse reactions, damage the kidneys in patients with already reduced kidney function[98]. Increases the risk of neonatal death in pregnancy[99] and Gadolinium deposition is facilitated in the brain of animal models[100]. Additionally there were astrocyte damage evident upon Gd administration in the animals used as stroke-models[100]. Dentate nucleus and globus pallidus have been shown to retain Gd[101] with unknown long term significance. There are some studies on the Gd use and reduced white blood cell count[102], neurotoxicity[103] summarized in[104].

Therefore, non-invasive modalities like APTw may have a larger role to play in the clinical setting due to repeat exposures to MRI examinations in brain tumor patients for presurgical evaluations and follow up.

Material and Methods

Patients

For Papers I and II, inclusion criteria were age above 18 years, suspected with primary or secondary neoplasm (Figures 2-5). There was an overlap of patients classified by WHO 2007 guidelines[105] for classification of tumors and the 2016 classification[11] and ultimately the 2007 was chosen as the 2016 did not exist when these two studies commenced, nor did the original study from which Paper I-II are sampled from. For Papers III-IV, inclusion criteria were age above 18, suspected neoplasm WHO grade 1-4 or brain metastasis. For papers III-IV the division of LGG into WHO grade 1-2 and WHO grade 3-4 into HGG, was kept according to the 2007 WHO classification. The molecular markers, brought up in the 2016 classification, for each entity are accounted for in original Table 1 for paper III. For Paper IV and glioblastoma, no stratification based on IDH-expression was made.

Paper I

This study included a sub cohort of 60 patients out of a larger cohort of 114 patients included from a related longitudinal study of primary and secondary brain tumors with eligibility criteria: above 18 years of age and presenting with space-occupying lesion(s) suspected to represent primary or secondary brain tumors, and after given informed consent. As these 60 were selected from the initial pool of patients, 17 were excluded due to being highly suspicious of meningioma (upon segmentation confirmed by histopathology as meningioma), having lesions engaging skull and or having limited preoperative MR examinations, i.e., missing DWI or PWI. Of these 43 included 18 were labelled as HGG, 10 as LGG, and 15 as MET as shown in original Table 1 in paper I. 30 males and 13 females, Mean age at diagnosis 64 for HGG, 45 for LGG and 59 for MET.

Paper II

Similar as for paper I, in this paper 33 patients, above 18 years of age (10 MET, 9 LGG, 14 HGG) were selected as a sub cohort out of same larger cohort of 114 patients in a longitudinal brain tumor study and after given informed written consent were included for retrospective analysis of presurgical MR Spectroscopy exam, original Table 1 in paper II Note not all patients exhibited adequate quality on

obtained spectra, while not all patients exhibited every type of target tissue below the placed spectroscopy VOI (volume of interest). 11 females and 22 males, mean age at diagnosis for HGG 64 years, 57 years for MET, and 47 for LGG.

Paper III

This study included patients above 18 years old, presenting with a suspected brain lesion and given informed written consent. These patients underwent standard MRI protocol for brain tumor with T1, T2, FLAIR, Perfusion and Diffusion weighted imaging i.e., pre-, and post-contrast imaging that is the mainstay for tumor diagnostics internationally albeit with the addition of APTw imaging protocol. Age range 26-76 years, mean age of 55 years and 22 males, 4 females. 8 LGG, 2 MET and 16 HGG as initial cohort as all patients up until commencement of analysis were included. 2 LGG were excluded due to suspicion of progression and 2 MET as they were not quantitatively sufficient for further statistical analysis.

Paper IV

The study included 44 patients above 18 years of age and after given written consent. Seven (1 anaplastic astrocytoma, 6 glioblastoma) patients that had missing ATRX status were excluded, 2 Anaplastic Oligodendroglioma were also excluded as they are no longer an entity according to the latest WHO Classification (2016) of brain tumors. Three patients with anaplastic astrocytoma had ATRX expression immunohistochemistry analysis performed. As the low number did not allow for statistical subgroup testing, these were also excluded. Final cohort consisted of 32 patients, 26 males and 6 females. Mean age for ATRX-wt glioblastoma patients at obtained histology verification of tumor type was 59 years and 39 years for the ATRX-mut glioblastoma.

MRI Acquisition protocols

Paper I

A 3 T Siemens Healthcare MAGNETOM Skyra® (Erlangen, Germany), was utilized for paper I with a standard 20-channel head/neck coil. DSC, dynamic susceptibility contrast perfusion MRI; spatial resolution of 1.7; 1.7; 5.0 mm^3 and 1.5 s time resolution, single-shot gradient echo EPI-gradient sequence with echo-time of 27 ms. Diffusion weighted imaging DWI and Diffusion Tensor Imaging DTI were performed with diffusion sensitized single-shot echo planar imaging (SSEPI) by utilization of b-values ranging from 0 and 1000 s/mm^2 and 30 non-co-linear diffusion gradient directions. Spatial resolution was 2.0; 2.0; 2.0 mm^3. FLAIR; 2D fluid attenuated inversion recovery, TSE; T2 2D Turbo-Spin-Echo, T1 3D MPRAGE (Magnetization Prepared Rapid Gradient Echo) with pre and post

contrast Gadolinium (Gd) administration (Isotropic Resolution of 1 mm). Entire scan time 60 minutes.

Paper II

3 T Siemens Healthcare MAGNETOM Skyra® (Erlangen, Germany) with a 20-channel head coil was utilized for acquisition of Proton MRS (1H-MRS) Imaging data. Volume of interests (VOI) calibration for localization in the brain was done and obtained after Gd intravenous administration with FLAIR and T1-MPRAGE; TR of 1900 ms, TE of 2.5 ms for the T1w and TR, TI, and TE of 9000 ms, 2500ms, and 81 ms respectively. PRESS (Point-RESolved spectroscopy sequence with TR 2000 ms and TE of 144 ms) were used for acquisition of the 1H-MRS scans with a voxel size of 10; 10; 15 mm within a VOI of either the size 4;4;1 or 8;8;1 with regards to flexible placement depending on location/size/proximity to bone. Total scan time was 6 min and 12 seconds.

Paper III & IV

For these two papers, the examination protocol was identical. Patients underwent examination on a 3 T scanner (MAGNETOM Prisma, Siemens Healthcare, Erlangen, Germany). Conventional clinical protocol and sequences were used apart from the prototype APTw imaging sequence. Isotropic resolutions for pre and post Gd contrast T2 TSE 2D (turbo spin echo, FLAIR 3D, T1-3D MPRAGE were 1 mm for T1w and 3D FLAIR, 5 mm for the T2 TSE. A CEST (chemical exchange saturation transfer) imaging prototype sequence was obtained from the manufacturer (Siemens Healthcare) and utilized; 3D GRE (Gradient Echo) for acquisition of the Z-spectrum i.e., water saturation spectrum with 2.0;2.0;4.0 mm^3 and 22 slices. Reference image was unsaturated and labeled S0 and was acquired -150 ppm off-resonant presaturation frequency relative to that of water to suppress the macromolecular background signal. B1 was set to 2 μT, with 21 frequency offsets ranging from -610 to 610 Hz, in total 22 with the reference image S0. Five hyperbolic secant pulses (100 ms) and four interpulse delays (61 ms) made up the saturation module and total scan time was approximately 45 min.

Software and segmentation

Paper I

For this paper two programs were mainly used for postprocessing and segmentation of tissue/lesion; Nordic ICE (NordicNeuroLab, Bergen, Norway; http://www.nordicneurolab.com) and a MATLAB-based software Eval-Gui for segmentation (developed by Markus Nilsson, Lund University, Lund, Sweden). Nordic ICE was used to approximate the cerebral blood flow and blood volume in

the brains of the participants i.e., to calculate perfusion maps. Eval-Gui enables full segmentation with fully manual segmentation capabilities. It was used to fully segment the lesion on T1-MPRAGE Gd-enhanced maps, the entire hyperintensity abnormality on FLAIR, and to place ROIs on CBF and CBV maps. Necrotic, cystic, or hemorrhagic areas could be removed easily within the Eval-Gui. Pixels or voxels that were encircles with a ROI could be saved and the intrinsic value extracted from the corresponding maps. The measured ROI could easily be overlayed from quantitative map to map and were corrected and surveyed by a neuroradiologist P.C.S (original Figure 1 in paper I).

Paper II

LC Model software (LCModel version 6.3-1L, Steven Provencher, Ontario, Canada) was used for estimation of following metabolic biomarkers: N-Acetyl Aspartyl Glutamate, Creatine, Lactate, Phosphocholine, Myo-Inositol, Glutamine, Glutamate, Lipids, Glycerophosphocholine, macromolecules, phosphocreatine, for each 1H-MR spectrum obtained. Tissue within the MRSI VOI voxels was labelled according to morphological appearance i.e., non-contrast-enhancing tumor, contrast-enhancing tumor, cystic/necrotic tissue, perilesional edema, ipsilateral normal appearing white matter or contralateral normal appearing white matter. Non contrast enhancing tumor, and contrast enhancing tumor tissue was pooled together for LGG, HGG and MET due to the low amount of VOI after labelling. Heavy baseline distortions, poor Signal to Noise ratio present in spectra or presence of artifacts resulted in exclusions of just those spectra and not subjects in their entirety.

Paper III

Medixant. RadiAnt DICOM Viewer [Software], version 2020.1. Mar 9, 2020 (https://www.radiantviewer.com) was used for manual delineation of ROIs. APTw signals of highest intensity were identified on color maps and one ROI was drawn and copied over to T1-MPRAGE Gd enhanced images as to ascertain that the measurement or ROI was within the contrast enhancing part of lesion or in those instances where no enhancement was present, within area of hypointensity on T1w images corresponding to hyperintensities on FLAIR. Additionally, for reducing the bias within the chosen method with one ROI of 10 pixels, a whole-lesion ROI was drawn manually with utilization of 3DSlicer 4.11.0, Nov 1, 2020 (http://www.slicer.org/) for Supplemental S1 analysis.

Paper IV

Whole tumor segmentation was performed via, 3DSlicer version 4.11.2 (http://www.slicer.org/). Cystic or necrotic segments and large vessels were avoided

and subsequently removed during 2nd survey of measurements with a neuroradiologist with 20 years of experience (PCS).

Ethical permissions

Written informed consent was obtained from each patient for Papers I-IV. Papers I and II were approved by The National Ethical Review Board (#2011/598, 2011/14, 2012/188, 2014/368). Papers III and IV are part of the same research project which was approved by the National Ethical Review Board (#2016/531, #2017/866, #2018/993, 2020-00851).

Statistics

For papers I-IV normality plots were constructed in SPSS versions 23-26 (IBM Corp., New York, NY, USA; formerly SPSS Inc., Chicago, IL, USA). Shapiro-Wilk's test performed. Boxplots, skewness, kurtosis, and outliers were assessed before opting for further post hoc testing.

Paper I & Paper II

For paper I, SPSS v. 23.0 (IBM Corp., New York, NY, USA; formerly SPSS Inc., Chicago, IL, USA) was used for comparison of significant differences in biometric values for patients with LGG, HGG and MET. Kruskal-Wallis H test was used for multiple comparisons and followed up with pair-wise testing via Mann Whitney U test. Kaplan Meier Survival analysis with Log-Rank, Breslow, Tarone-Ware statistics were performed for overall survival. Bonferroni correction was utilized and corrected alpha set at $p < .016$ and ROC analysis and Logistic regression for predictive modeling of tumor type based on biomarkers CBF, CBV, ADC, volume of edema or tumor, the ratio edema volume to tumor volume. All values except volumetric data were normalized with normal appearing contralateral white matter values.

Similarly as for paper II after normality testing described above, SPSS v. 23.0 (IBM Corp., New York, NY, USA; formerly SPSS Inc., Chicago, IL, USA) was utilized for biomarker comparisons between tissue types and LGG, HGG and MET groups. Biomarkers and tissue types mentioned under 3.3 Software and segmentation were compared after Bonferroni correction here set at $p < .017$ with Kruskal Wallis H, Mann-Whitney U for testing of significant differences. Overall survival was probed with Kaplan Meier Survival analysis and ultimately a ROC analysis was performed with logistic regression on a combination of the statistically significant biomarkers for differentiation of MET/LGG/HGG.

Paper III

For this paper, SPSS v. 24.0 (IBM Corp., New York, NY, USA; formerly SPSS Inc., Chicago, IL, USA) was utilized for post hoc with Mann Whitney U testing after normality testing described above. LGG and HGG were evaluated for statistical differences in mean, max, min, and range APTw signal in the area/volume identified visually as having the highest APTw signal intensity on color maps. MET group were excluded due to insufficient numbers (n = 2). A logistic regression model with statistically significant parameters was constructed for significant parameters (mean, max, range APTw signal).

Paper IV

For this paper, SPSS v. 26.0 (IBM Corp., New York, NY, USA; formerly SPSS Inc., Chicago, IL, USA) was utilized. Testing for normal distribution as described above for papers I-III, with Mann-Whitney U as post hoc testing where glioblastoma with and without loss of ATRX were compared and analyzed across mean, median, and maximum APTw signal.

Results

Paper I

The diagnostically valuable parameters for differentiation between HGG and LGG were normalized ADC, CBF, CBV within tumor and CBF in edematous tissue which is also shown in the Table 4 in the original paper. For the differentiation of LGG and MET, normalized ADC, CBF, CBV within tumor, ADC in edematous tissue, volume of edematous tissue, ratio between the volume of edematous tissue to that of the tumor (Vol-E / Vol-T). ADC within edematous tissue was the only significant ($p < .014$) parameter for differentiation between HGG and MET, with the HGG exhibiting lower normalized ADC values in edema (1.49) with those of MET (1.85).

Table 1. ROC analysis output for distinguishing HGG and MET using biomarker normalized ADC in edema. AUC, biomarker cut-off, sensitivity (%), specificity (%) with 95% CI and P-values.

HGG/MET	nADC-E
AUC	.76
95 % Confidence interval	.58-.94
Cutoff-value	1.63
Sensitivity	68.8%
Specificity	80%
p-value <	.015

Normalized CBF in tumor, as a single biomarker, had the best predictive capacity between LGG and HGG (cut-off 4.12; $p < .001$) and LGG vs. MET (cut-off 4.35; $p < .001$) with 93.3% and 100%, sensitivity and specificity respectively (Tables 1-3). The combination of normalized ADC, CBF, CBV in tumor with CBF in edematous tissue ($p < .001$) performed 100% in sensitivity and specificity in predicting LGG vs. HGG, with a higher Area under the Curve AUC (1.00) and Confidence Interval CI (1.00-1.00) than that of normalized CBF in tumor as a single biomarker: .95 AUC, .86-1.00 CI (Tables 1-3). For LGG and MET, the combined approach of Vol-E, Vol-E / Vol-T, normalized ADC, CBF, CBV in tumor and normalized ADC in edematous tissue also performed better than normalized CBF in tumor with regards to AUC (.96 vs .95), CI (.88-1.00 vs .84-1.00) albeit the combined approach had similar sensitivity and specificity; 93.3% and 100% respectively, (Tables 1-3). Mean time to progression MTP had too few subjects for comparison between LGG

and HGG. Overall mean survival (OS) differed significantly for the three groups with Breslow ($p < .001$), Tarone-Ware $p < .01$ being significant in the Kaplan Meier Survival analysis for LGG (46.2 months), HGG (18.7 months), MET (20.1 months).

Table 2. ROC analysis output for distinguishing HGG and LGG using biomarkers.
AUC, biomarker cut-off, sensitivity (%), specificity (%) with 95% CI and P-values.
Combined biomarkers nADC-T, nCBF-T, nCBV-T, and nCBF-E. *Probabilistic cut-off

HGG/LGG	nADC-T	nCBF-T	nCBV-T	nCBF-E	Combined Biometrics
AUC	.87	.95	.91	.82	1.00
95 % Confidence interval	.73-1.00	.86-1.00	.79-1.00	.64-1.00	1.00-1.00
Cutoff-value	1.76	4.12	6.06	1.03	.50*
Sensitivity	85.7%	93.3%	80%	92.9%	100%
Specificity	80%	100%	90%	70%	100%
p-value <	.003	.001	.001	.009	.001

Table 3. ROC analysis output for distinguishing LGG and MET using biomarkers.
AUC, biomarker cut-off, sensitivity (%), specificity (%) with 95% CI and P-values.
Combined biomarkers Vol-E, Vol-E/Vol-T, nADC-T, nADC-E, nCBF-T, and nCBV-T. *Probabilistic cut-off

LGG/MET	Vol-E (mL)	Vol-E / Vol-T	nADC-T	nADC-E	nCBF-T	nCBV-T	Combined Biometrics
AUC	.81	.91	.90	.81	.95	.87	.96
95 % Confidence interval	.63–0.98	.80–1.00	.77–1.00	.63–1.00	.84–1.00	.74–1.00	.88–1.00
Cutoff-value	22.39	1.05	1.71	1.62	4.35	6.37	.60*
Sensitivity	73.3%	80%	86.7%	80%	93.3%	60%	93.3%
Specificity	90%	100%	90%	90%	100%	100%	100%
p-value <	.011	.001	.001	.010	.001	.002	.001

Paper II

The tumor tissue defined by merging non- and contrast enhancing VOIs differed significantly for LGG and HGG and metabolites tLip/tCho ($p < .004$) and Ins/tCho ($p < .004$) (Tables 4-6). Contralateral normal appearing white matter did not differ between MET, LGG, HGG. For ipsilateral normal appearing white matter tissue and comparison across HGG vs. MET and metabolites tCho/tCr ($p < .015$) and NAA/tCho ($p < .017$) while tCr/tCho in edematous tissue was found to differ significantly ($p < .013$). LGG vs MET differed across non- and contrast-enhancing tissue for tLip/tCho ($p < .001$) and Ins/tCho ($p < .001$) (Tables 4-6). The constructed logistic regression model with combined metabolites for HGG/LGG outperformed the AUC and CI for the single metabolites while matching 100% sensitivity for the

single metabolite Ins/tCho and specificity of 100% for tLip/tCho, as evident by the ROC analysis (Original Figures 3-5 in paper II, Tables 4-6).

Table 4. ROC analysis output for distinguishing HGG and LGG using MRS metabolites.
AUC, Metabolite cut-off, sensitivity (%), specificity (%) with 95% CI and P-values. *Probabilistic cut-off

HGG/LGG	tLip - tCho	Ins - tCho	Combined Biometrics
AUC	.905	.905	1.00
95 % Confidence interval	.746-1.0	.767-1.0	1.0-1.0
Cutoff-value	2.35	1.61	.499*
Sensitivity	83.3%	100%	100%
Specificity	100%	75%	100%
p-value <	.004	.004	.001

Table 5. ROC analysis output for distinguishing HGG and MET using MRS metabolites.
AUC, metabolite cut-off, sensitivity (%), specificity (%) with 95% CI and P-values. *Probabilistic cut-off

HGG/MET	tCr - tCho	tCho - tCr	NAA-tCho	Combined Biometrics
AUC	.824	.788	.817	.935
95 % Confidence interval	.647-1.00	.567-1.00	.634-1.00	.825-1.00
Cutoff-value	2.65	.37	.80	.311*
Sensitivity	77.8	75	75	100
Specificity	76.7	84.6	84.6	81.8
p-value <	.013	.030	.017	.002

For HGG and MET, the combined metabolite model with tCr/tCho in edematous tissue and NAA/tCho from ipsilateral normal appearing white matter, exhibited higher AUC and CI as well as higher sensitivity of 100% but lower specificity of 81.8% as NAA/tCho showed higher specificity 84.6% (Tables 4-6). Combining tLip/tCho and Ins/tCho measured in non- and contrast enhancing tissue in LGG and MET showed equal sensitivity and specificity as tLip/tCho i.e., 100 % sensitivity and specificity, and identical AUC of 1.00 and CI of 1.00-1.00) (Tables 4-6).

Table 6. ROC analysis output for distinguishing LGG and MET using MRS metabolites.
AUC, Metabolite cut-off, sensitivity (%), specificity (%) with 95% CI and P-values. *Probabilistic cut-off

LGG/MET	tLip - tCho	Ins - tCho	Combined Biometrics
AUC	1.00	.984	1.00
95 % Confidence interval	1.00-1.00	.935-1.00	1.00-1.00
Cutoff-value	3.59	1.69	.50*
Sensitivity	100%	85.7%	100%
Specificity	100%	100%	100%
p-value <	.001	.001	.001

For Overall Survival OS, there were significant differences between HGG, LGG and MET i.e., 17, 8 and 29 months, respectively ($p < .009$ Tarone-Ware). Additionally, stratifying LGG/HGG/MET across Ins/tCho, where all VOIs in the affected hemisphere were pooled together, equal/below, or above 1.29, showed those brain tumors with 1.29 or below had a significantly lower survival (Original Figure 2 in paper II)

Paper III

Mean, max and range APTw% signals were found to be significant biomarkers for differentiation of LGG and HGG, p-values = .005; .002; .033, respectively. Minimum APTw% signal was not found to be significant. Cut-offs in APTw signal: 1.90%, 2.48%, .91% resulted in sensitivity / specificity of 93.8% / 83.3% for mean, 93.8% / 100% for max and 93.8% / 83.3% for range (Table 7).

Table 7. ROC analysis output for distinguishing HGG and LGG using APTw signal intensity.
AUC, APTw signal cut off (%), sensitivity (%), specificity (%) with 95% CI and P-values. Mean, max, range & combined biomarkers from logistic regression model. *Probabilistic cut-off value generated by model.

Variable	Mean/Max	Range	Combined
AUC	.896 / .948	.802	.958
95 % Confidence interval	.751-1.0 / .846-1.0	.523-1.0	.873-1.0
Cutoff-value	1.90% / 2.48%	.91%	.38*
Sensitivity	93.8% / 93.8%	93.8%	93.8%
Specificity	83.3% / 100%	83.3%	100%
p-value =	.005 / .002	.033	.001

The logistic regression model with the combined biomarkers mean, max and range of APTw signal showed in the ROC analysis; higher AUC = .958 and CI of .873-1.00 than max APTw% which was the best single biomarker with AUC of .948, CI of .846-1.00. The combined approach matched the max APTw% signal's sensitivity

and specificity of 93.8 and 100% specificity in the differentiation of HGG from LGG (Table 7).

MGMT promoter methylation status and IDH status could not be predicted due to insufficient numbers for statistical analysis or due to post hoc tests being non-significant with p-value > .05 for all mean, max, min, and range APTw% signal. The radiological diagnosis upon when patient presented with symptoms and underwent MRI, was retrospectively assessed. Out of 26 patients: a total of 6, 8 and 12 were diagnosed tentatively as MET, HGG and LGG, respectively (Table 8). In total 8 out of 26 were mislabeled by the initial radiological classification. For the reader assessment 6 patients had to be excluded due to known tumor type by reader 1, 2 or 3 and progression from LGG to higher grade tumor. The prospective analysis with readers 1, 2 and 3 diagnosing the remaining 20 patients, after exclusions, mounted to 80%, 80% and 65% correct diagnosis, respectively. Max APTw% signal correctly classified 21 out 22 glial tumors, MET were excluded due to insufficient numbers (n = 2) for the classification with APTw. Similarly, mean APTw% signal also classified 21 out of 22 correctly (Table 8). Comparing the classification logistic regression models in the Supplementary Material S1, the combination of mean and maximum APTw% signal (Whole Tumor ROI) vs. the combination of mean, maximum and range (10 Pixel ROI within tumor) both models misclassified 3 subjects out of 24 in total.

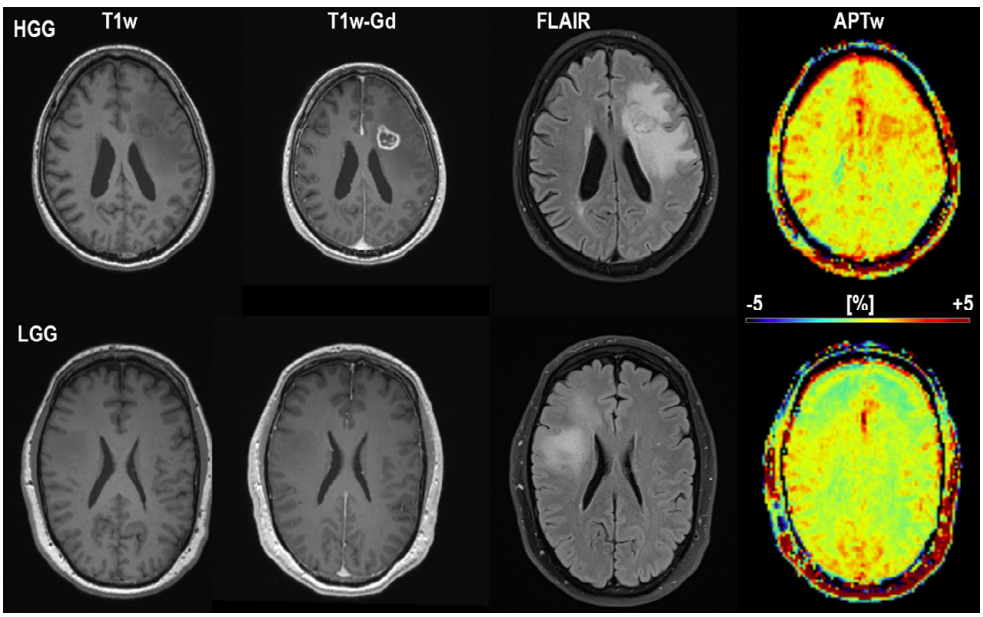

Figure 8. Difference in APTw% signal in HGG vs. LGG
Conventional MRI; T1-MPRAGE without contrast, T1-MPRAGE with Gadolinium, FLAIR and APTw in color for one subject exhibiting a high grade glioma and one patient with a low grade glioma. Of note is the increased APTw% signal in the HGG vs. the LGG, shown on APTw color maps.

Table 8. Diagnosis of brain lesions into HGG/LGG/MET at primary presentation of disease and follow-up review with 3 readers and quantified intralesional mean APTw signal with cut off >+2.0%.
*Incorrect classification with misdiagnosis within parenthesis, ** Were not assessed by reviewers due to known tumor type, *** Excluded due to radiological progression after obtaining histological sample, **** APTw-Mean of > +2.0% enabled correct diagnosis, *****APTw-Mean of <+2.0% did not enable correct diagnosis, HGG = High grade glioma, LGG = Low Grade Glioma, MET = Metastasis.

Subject/Initial radiological classification	Reader 1	Reader 2	Reader 3	Classification with APTw mean > +2.0%
1/Correct HGG	Incorrect (MET)*	Correct	Incorrect (MET)*	Correct
2/Correct HGG	Correct	Correct	Correct	Correct
3/Correct LGG	Correct	Correct	Correct	Correct
4/Incorrect (LGG)* HGG	Correct	Correct	Correct	Correct
5/Correct HGG	**	**	**	Correct
6/Incorrect (MET)* HGG	**	**	**	Correct
7/Correct HGG	**	**	**	Incorrect (LGG)*****
8/Correct HGG	Correct	Correct	Correct	Correct
9/Correct LGG	Correct	Correct	Correct	Correct
10/Incorrect (MET)* HGG	Correct	Correct	Correct	Correct
11/Correct LGG	Incorrect (HGG)*	Incorrect (HGG)*	Incorrect (HGG)*	Incorrect (HGG)****
12/Correct LGG	***	***	***	***
13/Incorrect (MET)* HGG	Incorrect (MET)*	Correct	Correct	Correct
14/Correct LGG	Correct	Incorrect (HGG)*	Incorrect (HGG)*	Correct
15/Incorrect (LGG)* HGG	Correct	Correct	Correct	Correct
16/Correct LGG	***	***	***	***
17/Correct LGG	Correct	Correct	Correct	Correct
18/Incorrect (LGG)* HGG	Correct	Correct	Correct	Correct
19/Correct HGG	**	**	**	Correct
20/Correct HGG	Correct	Incorrect (MET)*	Incorrect (MET)*	Correct
21/Correct HGG	Correct	Correct	Correct	Correct
22/Incorrect (MET)* HGG	Correct	Correct	Correct	Correct
23/Incorrect (LGG)* HGG	Incorrect (LGG)*	Correct	Incorrect (LGG)*	Correct
24/Correct LGG	Correct	Correct	Correct	Correct
25/Correct MET	Correct	Incorrect (HGG)*	Incorrect (HGG)*	Excluded
26/Correct MET	Correct	Correct	Incorrect (HGG)*	Excluded

Paper IV

The final cohort was comprised of 32 patients with glioblastoma (GB; n=32). APTw% signals: mean, median and max were analyzed on (GB) that was stratified across ATRX-expression status into two groups (ATRX-wt = 26, ATRX-mut = 6). Max APTw% signal was the sole discriminant with p = .023 for GB (Figures 9-10, Table 9). Mean and median APTw% signal did not differ significantly for GB across ATRX-expression status with p-values = .83 and .65 respectively (Figure 9)

Table 9. Summarized ROC-analysis
ROC analysis for distinction between ATRX-mut from ATRX-wt glioblastoma (N = 32) utilizing APTw max signal

Variable	Output
Area under the Curve	.802
95 % Confidence interval	
Lower Bound	.651
Upper Bound	.952
Cutoff-value	3.83%
Sensitivity	100%
Specificity	69.2%

ROC analysis of max APTw% signal showed the same cut-off of 3.83% was the most optimal to use GB in differentiation of those with lost ATRX status: ATRX-mut, and those with intact ATRX-wt. The analysis showed across GB (n = 26 ATRX-wt, 6 ATRX-mut, total 32 subjects) showed AUC = .801, sensitivity of 100% and specificity of 69.2% (Figure 10, Table 9). Age differed significantly for GB when analyzing date for the primary histology analysis obtained (59 years vs 39 years for ATRX-wt GB and ATRX-mut GB) p-value = .008. Although age differed significantly for the ATRX-mut vs ATRX-wt subjects, overall survival did not differ significantly between the ATRX-mut and ATRX-wt GB (21 weeks vs. 19 weeks).

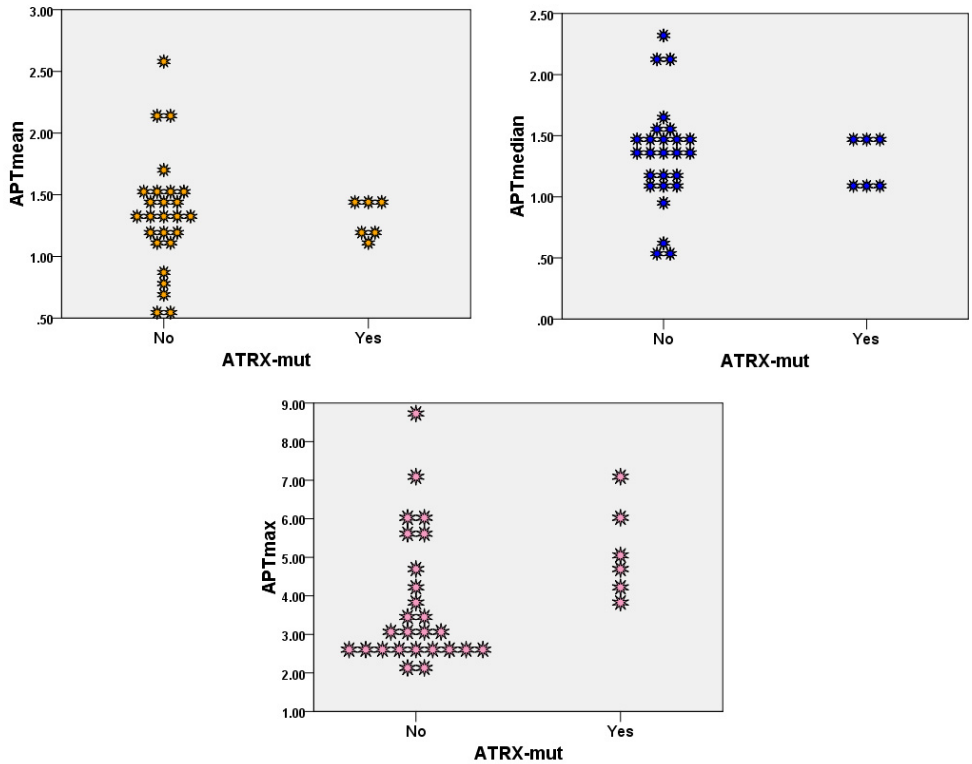

Figure 9.
2D-plots for APTw % mean (top left) p = .83, median (top right) p = .65 and (bottom) max signal for ATRX-wt and ATRX-mut glioblastoma. Max APTw% signal p-value = .023

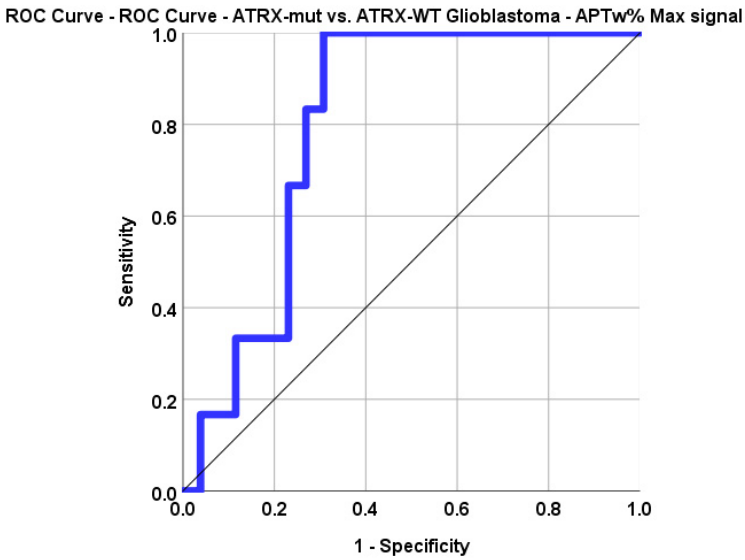

Figure 10.
ROC-curve for APTw% max signal for glioblastoma. Mann Whitney-U test p-value = .023. AUC = .801, p-value = .023 for ROC-curve. Asymp. 95% CI .651-.952. Max-signal Cut-off of 3.83% results in 100 sensitivity and 69.2 % specificity for ATRX-mut n = 6, ATRX-wt n= 26.

Discussion

Papers I-II

In paper I, an effort was made to predict, from a mixed cohort of WHO grade 3 and grade 4 glioma (HGG), WHO grade 2 glioma (LGG), and metastasis (MET). Additionally, the MET group was also relatively heterogeneous in terms of type of histological cancer. As previous efforts to discern these types of brain tumors had varied success[106–108], the hypothesis of utilizing perfusion, diffusion, volumetric biodata from different types of tissues in the brain arose. These areas and tissues were identified as the lesion itself, the edematous tissue adjacent to the lesion and the normal appearing white matter tissue in the contralateral (relative to tumor) hemisphere. Other studies have tried utilizing necrosis, edema, lesion, total volume for differentiation of LGG/HGG/MET[108–113] Other efforts to solve the diagnostic problem for molecular correlations with supervised/unsupervised machine learning algorithms and/or radiomic feature extraction from conventional Gd enhanced imaging i.e., T1- and T2w MRI, have been made[114,115].

As the number of input variables in the models increase, there was a risk of overfitting the model and inferring bias as the input information is static, i.e. non statistically significant data[116]. For papers I-II (and paper III) the number of input variables never surpass the number 6 in total for the models. Hence, the constraints did not just occur naturally, as there are constraints for the logistic regression as an algorithm as well in terms of optimal number of input variables[116,117]. For example, in paper I the distinction between LGG and MET had the most and only significant biomarkers incorporated in the logistic regression model (six in total) therefore more variables could not be added to the model due to p-value > chosen level of alpha. The biomarkers: Volume of edematous tissue, the ratio between the edematous tissue and tumor volume, the normalized blood flow, blood volume within tumor and the apparent diffusion in tumor and edematous tissue combined (Vol-E, Vol-E/Vol-T, nADC-E, nCBF-T, nCBV-T, nADC-T) were the only significant biomarkers. By minimizing the number of variables in the multivariable model, you increase the likelihood of generating a numerically stable model which is also a way to ensure more straightforward implementation or usage of the model[116]. It is advisable to keep the number of input variables low while increasing the number of patients[118,119]. There exists also a need to choose the presumable best predictors or to experimentally determine which of the biomarkers in combination creates the best model for distinction[116]. However, we have been satisfied in choosing only the

significant biomarkers from univariate statistical setting with a p-value set at a maximum of .05. Furthermore, others have either chosen to incorporate all biomarkers without taking into account if the difference between the binary outcomes is by chance or not, i.e., significance level > .05[116]. Others have suggested that one can use a more liberal cut-off for the significance level and include all biomarkers that are p-value < .10 instead of alpha at .05 or less[118]. The methodology of choosing all variables available as input variables in the model confers the risk of "overfitting" which produces unstable numerical estimates through large standard errors, as one example[116]. Papers I-III produced probabilistic cut-off values of .50-.60 for paper I, .499, .311, .50 for paper II and .38 for paper III. Choosing a low number of variables to input into the logistic regression multivariable model is therefore even more important when dealing with smaller cohort sizes; this to avoid creating an overfit and unstable estimation by the model[116,117].

Harrell F., et al[117] argue that the more liberal significance level of maximum .20 to .25 may hold an advantage over p < .05 with risk of excluding advantageous biomarkers or variables from the model. Our reasoning in this regard was that for a physiological model to be constructed in an optimal way, the initial univariate analysis needed to establish a significant difference with alpha set at maximum of .05 for the quantified biomarkers or MRI signals across the different modalities. Therefore, the initially theorized biomarkers were carefully assessed before inclusion into the model and the set alpha level was a way of ensuring exclusion of variables differing by chance. Harrell et al.[117] suggest it may hold an advantage to contrast the multivariate logistic regression model with all variables at significance level set at p-values .20-.25, with the model based just on variables at alpha < .05. Variables changing in magnitude by tabulated values above 20% between primary and secondary model should be noted. These may indicate that even though they are not statistically significant in terms of the outcome measured (e.g., the non-significant biomarker normalized CBF for differentiation of HGG and MET in paper I) they can still contribute an important and substantial effect to the model's predictive capacity[117].

One area which would have added further depth to paper I-III is external validation of the constructed logistic regression models. The external validation is considered adequate to test any model[117]. If the model fails the external validation, then overfitting is a probable cause as it has been shown to be one of the most frequent causes for this failure[117]. There are other types of assessments which can be performed on the original dataset, i.e., internal validation[117]. This can either be performed by bootstrapping, cross-validation or data-splitting[117]. These types of validation could have potentially increased the value and generalizability of our models[117], if they had been performed.

For Paper I, the assumptions that governed our choice of variables as input to the models were based on the brain tumor's natural course or cycle in the brain of the patients. The biology and phenotype behavior separating those tumors that are to a

lesser degree malignant from those that are of a higher degree malignant was the main hypothesis. For example, the tumors have been modelled to elicit multiple cycles of neovascularization, necrotic center with the surviving viable tumors mostly localized near matured vessels and distal from the central areas of the lesion[120]. Other studies have utilized CBF, CBV, ASL, DWI, DKI, DTI, MRS and APT[108,109,111,112,121–125]. Diffusion weighted imaging DWI and ADC has been utilized as a biomarker for cellular density[28]. DSC-MRI (Dynamic susceptibility contrast enhanced MRI), DCE MRI (Dynamic contrast enhanced MRI)[108,111], ASL have been through measurements of cerebral blood flow (DSC, DCE, ASL) and volume (DSC, DCE) used as surrogates for vascular proliferation[28] as was Mean transit time MTT, a feature of DSC-MRI[28]. DTI and fractional anisotropy have been used as markers for white matter tract integrity[47–49].

The underlying background to paper I was that we would be able to create a model with logistic regression combination of the most relevant biodata: level of white matter tract integrity (FA)[47–49], cellularity (ADC), edema and tumor volume (conventional MRI volumetrics), vascular proliferation (CBF, CBV) within lesion and in perilesional edematous tissue[28]. The differences in behavior regarding MET and HGG that we tried to take advantage of were vasogenic edema (MET) and propensity to infiltrate into grey matter[28,126]. However, even despite inherent differences in grey matter vs. white matter in normal brains in terms of ADC[127] no significant differences were found within the tumor for MET and HGG. However, there was a significant difference in the perilesional edematous tissue by utilization of ADC. The potential alterations of white matter tracts are elucidated in, with deviation, edema, infiltration and destruction all altering both FA and ADC by extension[128]. They hypothesized that in comparison with MET the glioblastomas assert greater deviation, infiltration and destruction than MET on the tracts[128]. As suggested by[28,43,58,129] ADC was lower in HGG vs MET, likewise in Paper I the median normalized ADC in edema was lower in HGG 1.49 vs. 1.85. In retrospect, it would have perhaps been more suitable according to[117], to incorporate Vol-E / Vol-T into a multivariable logistic regression model as this biomarker had a p-value < .109 and as METs usually have more vasogenic tissue edema than glioblastoma[28,43,52,58,129,130].

Likewise, for paper II, the lesions in the brain were stratified based on their morphological appearance: edematous tissue, non- and contrast-enhancing tumor, cystic and or necrotic tissue, relative to tumor ipsilateral or contralateral normal appearing, on T1w-Gd enhanced imaging, white matter.

Figure 3 in the original paper II summarizes the main biometrics incorporated in the logistic regression model: tCr/tCho in edematous tissue and tCho/tCr and NAA/tCho in the ipsilateral normal appearing white matter i.e., the normal appearing white matter tissue adjacent either to tumor or perilesional edema as identified on T1w-Gd enhanced imaging. Perilesional Cho-Cr ratios were found to be elevated[28,58], whilst Cho/NAA ratios reduced according to[28,123] in glioblastoma.

These were deemed hallmarks of increased cellular density due to increased infiltration[28,123].

In Paper II it was shown that MET had higher tCho/tCr (.39) and NAA/tCho (2.43) than HGG (.34 and 1.14, respectively) in the ipsilateral normal appearing white matter. MET had also higher tCr/Cho (2.95) than HGG (2.43) measured in the edematous tissue, which is more in line with Ch/Cr ratio having lower values in MET than glioblastoma[28,123].

Also evident in the original Table 4 in paper II, several additional biomarkers may have been used in the multivariable logistic regression model had there a less conservative significance level of alpha been utilized according to the suggestions of[116]. For LGG vs HGG differentiation, Ins/tCho ($p < .02$) in edema, tCr/tCho ($p < .018$) in contrast enhancing tissue, tCho/tCr ($p < .169$) in contralateral normal appearing white matter these could have been incorporated as well. The motivation for keeping the number of predictors or biomarkers as low as possible has always been as to minimize bias, produce a model with low numbers of confounding elements to sustain the stability of the model[117], the estimated standard errors as low as possible and minimize the dependency of the model on the quantified biomarkers[116].

Another issue with spectroscopy, which was encountered in paper II, is the heterogeneity in missing data. Several metabolites had to be excluded due to non-adequate quality of obtained spectra. The missing data can pose extra issues when building models as to high frequencies of missing data can render the model inaccurate[117]. For our cohort, the missing data was not of a high frequency, nor threatening the accuracy, although our dataset was fairly small, which also increases the risk of inserting inaccuracies into the model[117].

High grade gliomas (WHO grade 3-4 glioma) have previously been established to have higher proliferation, more rapid growth and hypoxic and necrotic areas to a higher extent than LGG (WHO grade 1-2 glioma)[28,108,111]. Leaky capillaries due to abnormal changes in the capillary endothelial permeability, increased numbers of vessels per volume unit brain tissue are characteristics of HGG[28,79–81]. This inherent biological difference between LGG and HGG can be utilized for differentiation through perfusion weighted imaging to stratify glioma across WHO grades 1-4[28,131–134]. In Paper I significant differences between LGG and HGG were found in perilesional edematous tissue (normalized CBF, p-value $< .008$), viable tissue tumor without necrotic or cystic elements (normalized CBV, CBF and ADC, p-values $< .001$, .001, .002, respectively).

Similarly, for paper II, stratification by tissue type was explored and expanded upon in terms of that the normal appearing white matter in both hemispheres was probed for metabolic differences that would aid in the differentiation of LGG from HGG. MR spectroscopy has previously been shown to help in the differentiation of LGG and HGG tumors[28,122]. The multivariable model for differentiation of LGG/HGG in

Paper II was constructed by utilizing tLip/tCho ($p < .004$), Ins/Cho ($p < .004$) within contrast enhancing tissue (note that the contrast enhancing tissue VOIs were pooled together with the non-enhancing VOIs for both LGG and HGG). Several studies have showed Cho/Cr ratios are increased in HGG[28,135–138]. Others have shown a combined approach of MR spectroscopy, diffusion and perfusion weighted imaging may improve accuracy in prediction of WHO grade 1-4 glioma[28,139–142]. In paper II, emphasis was given to sole MRS exploration of tissue and the creation of a model with sole metabolic biodata. As shown in the original figure 4 in paper II, distinction could be achieved with high sensitivity and specificity for LGG and HGG with AUC of 1.00. For validation purposes it is important to note the biomarkers that were between chosen alpha .017-0.25 as suggested per[116]. Ins/tCho in edematous tissue ($p < .020$), tCho/tCr in non- and contrast enhancing tissue ($p < .151$) and contralateral normal appearing white matter ($p < .169$) as well as tCr/tCho in non- and contrast enhancing tissue ($p < .018$) may therefore serve as important biomarkers for further optimization of the constructed model for differentiation of LGG and HGG.

Paper III

In contrast to Papers I-II, for paper III a rather novel technique and modality, APT, was utilized for radiological evaluation of brain tumors. All included patients obtained their initial radiological diagnosis retrospectively reviewed after quantification of APTw mean ($p = .005$), minimum ($p = .055$), maximum ($p = .002$) and range ($p = .032$) APTw% signal. Max APTw% signal matched the sensitivity and specificity of the multivariable logistic regression model. AUC and 95 % confidence interval CI were higher for the model than the best predictor max APTw% with quantification by 10-pixel ROI. The CI was also higher for the model when whole tumor ROI was utilized, albeit with identical AUC (.896) as max APTw% and lower 81.3% sensitivity vs. 93.8% for max signal. Specificity was higher for model 100% vs. 83.3% for max APTw% signal. As higher AUC signifies a random subject or object sampled from group 1 is correctly classified with a higher probability than if a random object or subject had been sampled from group 2[143–147]. For paper I, the combined multivariable logistic regression model showed a higher AUC for HGG/LGG (1.00) and LGG/MET (.96) which was greater for any single biomarker. For paper II, HGG/LGG (AUC = 1.00) and HGG/MET (AUC = .935) was higher than rest of single metabolic biomarkers. However, LGG/MET exhibited equal AUC of 1.00 for the combined model and tLip/tCho quantified in non- and contrast enhancing tissue. With equal or higher probability of correctly classifying random objects from one group, the argument that the combined biomarker method with logistic regression may be the superior choice compared with choosing single biomarkers.

Even though the comparison with paper III cannot be considered optimal due to the exclusion of patients with metastases, the results show that APTw imaging may outperform the radiologists' and readers' assessment in separating the more malignant tumors from those of lesser malignant phenotypes i.e., WHO grade 1-2 glioma. As most subjects presenting with a metastatic lesion in the brain already have an established primary tumor, it can be suggested that this differentiation from gliomas can be slightly aided with a thorough patient history, apart from the imaging. Regrettably, a small error is present in the conclusion section of Paper III, where sensitivity and specificity ought to be 93.3% sensitivity and 100% specificity, with equal sensitivity and specificity for the single biomarker max APTw% signal, albeit with higher AUC and CI, suggesting the predictive accuracy to be higher in the combined multivariable model, and thus making it the superior approach in this cohort.

Paper IV

To our knowledge, paper IV will be the first study publishing the successful correlation of a MR imaging modality to ATRX expression status obtained by immuno-histochemistry in glioblastoma[125]. With the advent of new 2021 tumor classification from WHO[18], molecular typing with MRI correlations to histopathological gene expression has become of greater importance. For example IDH1 mutations in glioblastoma have previously been correlated to prolonged survival[28,148]. Another genetic expression correlated to prolonged survival through increased response to temozolomide TMZ therapy is MGMT promoter methylation status, with methylation being associated with aforementioned responses[28,149]. Unmethylated MGMT promoter has been correlated to ring enhancement on T1w Gd-enhanced imaging[28,150]. Utilization of other non-invasive techniques such as DWI (ADC) and perfusion (CBV) have not resulted in consistent findings for stratification of glioblastoma multiforme across MGMT promoter status[28,151–154].

Even if no overall survival benefit was observed between the ATRX-mut versus ATRX-wt in paper IV, the molecular characterization has been suggested to become of great importance for targeted therapies[155]. ATRX alterations overlap with TP53 alterations, they are proposed to be part of hot spot genetic alterations that may set of glioblastoma into a distinct pathogenetic behavior[155,156]. It is suggested that APTw imaging offers a noninvasive method for stratification of ATRX-mut glioblastoma from those being ATRX-wt.

Clinical impact

Papers I-IV clearly show that algorithms such as logistic regression can help increase accuracy in diagnosis of brain tumors. By combining data from conventional MRI techniques with novel techniques such as amide proton transfer imaging and utilizing the information from the brain tumors natural disease progression, models can be built which can improve the diagnostic accuracy by helping the radiologists in their decision making. In tougher diagnostic cases where correct diagnosis might be obtained late relative to other patient diagnoses, the utilization of algorithms which enable the user to use multiple imaging biomarkers may be of value at the clinic. These findings, along with the findings published for the past 15 years regarding amide proton transfer imaging, are now pushing the radiologist to:

1. Utilize previous modalities and their data in new ways
2. Incorporate new modalities such as APT in the clinical setting.

New, user friendly software for quantification of APTw MRI is already on the market and will be evaluated in our future research setting. An additional potential impact this work has brought on is the need for automated segmentation and presentation of diagnostic data. The heterogeneity in the malignant glioma can be exploited for diagnostic purposes but needs to be done in a less time-consuming manner. For papers III-IV it is clear that APT improves diagnostic accuracy in discerning less malignant from more malignant brain tumors. The modality can be utilized by radiologists with placement of one single measurement but also quantification of the entire lesion. Additionally, paper IV shows that APT can be used to stratify the most malignant gliomas across ATRX expression, opening the door for further advancement of research aiming to correlate MRI imaging biomarkers with those already established in the histopathological setting.

Future perspectives

All future perspectives encompass implementation of Amide proton transfer imaging in clinical practice. The APT as an imaging modality is currently undergoing a standardization as efforts on an international level among colleagues with interest in CEST and APT imaging to in consensus present and implement one APT sequence, as opposed to the many sequences that exist today. This will in turn ease validation efforts nationally and internationally.

1. Correlate biopsies with histology and protein analysis and quantitative APTw imaging from areas of low and high APT signal. Together with the neurosurgical department at Skåne University Hospital and Dr. Johan Bengzon, there is a great desire to take the next big step in bridging the gap between research sequence, histology, proteomics, and the clinic.

2. Implement and investigate the usefulness of APTw imaging in children and adolescents. APTw imaging being a completely non-invasive technique for imaging, one area of interest is pediatric brain tumors. Children with brain tumors often undergo several MRI sessions with (Gadolinium) Gd-based imaging techniques. Multiple exposures to Gd increases the risk of developing kidney damage, especially in those with established renal disease such as end-stage renal disease, chronic kidney failure grade 4 or 5[157]. APTw imaging may act as a future complementary modality to imaging in pediatrics, to help reduce exposure to Gadolinium. We have ethical approval for this study (#2018/444).

3. Implement CE-approved software at our clinic to aid neuroradiologists in the diagnosis of brain tumors.

4. To validate the existing models by testing these on external cohorts would be another step to move the APT sequences into clinical routine in brain tumor imaging,

Conclusions

Paper I

Combining several MRI modalities and utilizing quantified data from different types of tissue may improve accuracy in prediction of MET/LGG/HGG.

Paper II

By dividing brain tumors morphological appearance may yield valuable diagnostic information for distinction of LGG/HGG/MET. By stratifying the lesion into edematous tissue, necrotic/cystic, normal appearing white matter in ipsilateral and contralateral to tumor hemisphere and as viable tumor tissue exhibiting contrast enhancement or hypo-intensity on T1w Gd enhanced imaging, 1H-MRS may provide metabolic biomarkers capable of distinguishing LGG/MET/HGG.

Paper III

Amide proton transfer imaging is a valuable addition to the clinical setting. The modality shows promise in distinguishing LGG from HGG based on max, mean and range APTw% signals utilized separately as biomarkers or as variables in a multivariable logistic regression model, which showed higher predictive accuracy with higher AUC than the separate biomarkers, mean, max and range APTw% signal.

Paper IV

Amide proton transfer imaging can be a promising future tool for non-invasive stratification of ATRX-intact glioblastoma from those with loss of ATRX expression. Providing an interesting prospect and valuable non-invasive future tool for personalized treatment.

Acknowledgments

I wish, first of all to express deep gratitude to my family**, Dzevad, Samija, Dzana, Jasmina & Jakub Durmo.** Their relentless support, even before I embarked on this quest for knowledge, has been the shining light in my darkness. As I walked the stairs of the achievements of my predecessors, it became very clear, when my small pair of stairs were chiseled out, it was only to be with the help and support of family, friends, and colleagues. Special thanks to **Husein, Suvada and Vedad Canic and my friends** for your support as well.

My **main supervisor Prof. Pia C. Maly Sundgren** has been everything you can ask for in a supervisor. Even more so on a human level. Her understanding, devotion to science, medicine and to the hospital and clinic as organizations have been a deep inspiration for me, the student. I guess all of us that embark on the quest for knowledge, remain students in some respects. My most sincere thanks for helping me navigate, steadying the course across the vastness. Thank you for the opportunity to study under one of the greats in radiology and medicine. I also want to extend special thanks to Dr. **Pavel Maly**, for valuable input, thoughts and acting the compass on those cloudy nights.

Prof. **Linda Knutsson** and Assoc. Prof **Johan Bengzon**, thank you for all the advice and support, helping me push through when I have gotten stuck.

Prof. **Isabella Björkman-Burtscher**, Assoc Prof. **Markus Nilsson**, Dr. **Jonas Svensson,** Prof. **Elisabet Englund,** Dr. **Anna Rydelius** thank you for all those meetings when I've gotten stuck, and you helped in moving the projects forward. Prof. **Peter CM van Zijl**, thank you for all valuable input, advice, and encouragement to push through the hardships.

Dr. **Krister Askaner**, Dr. **Anna Rydhög, Mrs. Annika Törling-Ring** I am very grateful for all your help and encouragement during my PhD-studies.

Last but not by any means least, I want to thank Dr. **Jimmy Lätt**. Apart from Prof. Sundgren, I cannot think of anyone that has dedicated more of his time and effort in these projects and in me as a student. Words cannot describe the gratitude and level of indebtedness I feel. Thank you for providing me the hammer and chisel, when I set out with a wooden stick against this piece of marble.

References

1. Greenblatt, S. H. Harvey Cushing's Paradigmatic Contribution to Neurosurgery and the Evolution of His Thoughts about Specialization. *Bulletin of the History of Medicine* **77**, 789–822 (2003).
2. Bennett, A.H., Godlee, R. J. Case of cerebral tumour / by A. Hughes Bennett ; the surgical treatment by Rickman J. Godlee. | Wellcome Collection. *From Vol. LXVIII of the Medico-Chirurgical Transactions, published by the Royal Medical and Chirurgical Society of London, London : Printed by J.E. Adlard, 1885.* 33 (1885). Available at: https://wellcomecollection.org/works/tn95vhhj/items. (Accessed: 10th July 2021)
3. Kirkpatrick, D. B. The first primary brain-tumor operation. *J. Neurosurg.* **61**, 809–813 (1984).
4. Keen, W. W. The surgical treatment of intracranial tumors. *Faculty of Medicine of the University of Pennsylvania* 1–8 (1886). Available at: https://wellcomecollection.org/works/h7aqcdhj/items. (Accessed: 2nd August 2021)
5. Sandrone, S. & Zanin, E. David Ferrier (1843–1928). *J. Neurol.* **261**, 1247–1248 (2014).
6. Pearce, J. M. Sir David Ferrier MD, FRS. *J. Neurol. Neurosurg. Psychiatry* **74**, 787 (2003).
7. Bramwell, B. Intracranial tumours. *Edinburgh: Pentland.* 270 (1888). Available at: https://archive.org/details/intracranialtumo1888bram. (Accessed: 3rd August 2021)
8. Stoyanov, G. S. & Dzhenkov, D. L. On the Concepts and History of Glioblastoma Multiforme - Morphology, Genetics and Epigenetics. *Folia Med. (Plovdiv).* **60**, 48–66 (2018).
9. Martin-Villalba, A., Okuducu, A. F. & Von Deimling, A. The evolution of our understanding on glioma. *Brain Pathology* **18**, 455–463 (2008).
10. De Angelis, L. M. & Mellinghoff, I. K. Virchow 2011 or how to ID(H) human glioblastoma. *Journal of Clinical Oncology* **29**, 4473–4474 (2011).
11. Louis, D. N. *et al.* The 2016 World Health Organization Classification of Tumors of the Central Nervous System: a summary. *Acta Neuropathologica* **131**, 803–820 (2016).
12. Castillo, M. History and evolution of brain tumor imaging: Insights through radiology. *Radiology* **273**, S111–S125 (2014).
13. Abraham, T. & Feng, J. Evolution of brain imaging instrumentation. *Seminars in Nuclear Medicine* **41**, 202–219 (2011).

14. Adson, A. W., Ott, W. O. & Crawford, A. S. A Study of Ventriculography. *Radiology* **2**, 65–73 (1924).
15. Ferguson, S. & Lesniak, M. S. Percival Bailey and the classification of brain tumors. *Neurosurgical focus* **18**, (2005).
16. Scherer, H. J. A CRITICAL REVIEW: THE PATHOLOGY OF CEREBRAL GLIOMAS. *J. Neurol. Neurosurg. Psychiatry* **3**, 147–177 (1940).
17. Wen, P. Y. & Packer, R. J. The 2021 WHO Classification of Tumors of the Central Nervous System: clinical implications. *Neuro. Oncol.* **23**, 1215–1217 (2021).
18. Louis, D. N. *et al.* The 2021 WHO Classification of Tumors of the Central Nervous System: a summary. *Neuro. Oncol.* **23**, 1231–1251 (2021).
19. Ostrom, Q. T. *et al.* The epidemiology of glioma in adults: A state of the science review. *Neuro-Oncology* **16**, 896–913 (2014).
20. Shampo, M. A. & Kyle, R. A. Godfrey Hounsfield--developer of computed tomographic scanning. *Mayo Clin. Proc.* **71**, 990 (1996).
21. Ambrose, J. Computerized transverse axial scanning (tomography): II. Clinical application. *Br. J. Radiol.* **46**, 1023–1047 (1973).
22. Wolpert, S. M. Historical Perspective Neuroradiology Classics. *Am. J. Neuroradiol.* **20**, (1999).
23. Bradley, W. G., Waluch, V., Yadley, R. A. & Wycoff, R. R. Comparison of CT and MR in 400 patients with suspected disease of the brain and cervical spinal cord. *Radiology* **152**, 695–702 (1984).
24. Randell, C. P. *et al.* Nuclear magnetic resonance imaging of posterior fossa tumors. *Am. J. Roentgenol.* **141**, 489–496 (1983).
25. Brant-Zawadzki, M. *et al.* NMR demonstration of cerebral abnormalities: Comparison with CT. *Am. J. Roentgenol.* **140**, 847–854 (1983).
26. Brant-Zawadzki, M., Badami, J. P., Mills, C. M., Norman, D. & Newton, T. H. Primary intracranial tumor imaging: A comparison of magnetic resonance and CT. *Radiology* **150**, 435–440 (1984).
27. Taphoorn, M. J. B. *et al.* Neuro-radiology Imaging of brain metastases Comparison of computerized tomography (CT) and magnetic resonance imaging (MRI). *Neuroradiology* **31**, 391–395 (1989).
28. Berger, M. S. & Weller, M. *Gliomas. [Elektronisk resurs]*. (Elsevier, 2016).
29. Omuro, A. M., Leite, C. C., Mokhtari, K. & Delattre, J. Y. Pitfalls in the diagnosis of brain tumours. *Lancet Neurology* **5**, 937–948 (2006).
30. Eidel, O. *et al.* Tumor infiltration in enhancing and non-enhancing parts of glioblastoma: A correlation with histopathology. *PLoS One* **12**, (2017).
31. Zhou, J., Heo, H. Y., Knutsson, L., van Zijl, P. C. M. & Jiang, S. APT-weighted MRI: Techniques, current neuro applications, and challenging issues. *Journal of Magnetic Resonance Imaging* **50**, 347–364 (2019).
32. Newton, H. B. *Handbook of Neuro-Oncology Neuroimaging: Second Edition*. *Handbook of Neuro-Oncology Neuroimaging: Second Edition* (Elsevier Inc., 2016). doi:10.1016/C2013-0-19190-8

33. Basser, P. J. & Jones, D. K. Diffusion-tensor MRI: Theory, experimental design and data analysis - A technical review. *NMR in Biomedicine* **15**, 456–467 (2002).
34. Basser, P. J. New histological and physiological stains derived from diffusion-tenser MR images. in *Annals of the New York Academy of Sciences* **820**, 123–138 (Blackwell Publishing Inc., 1997).
35. Basser, P. J., Mattiello, J. & LeBihan, D. MR diffusion tensor spectroscopy and imaging. *Biophys. J.* **66**, 259–267 (1994).
36. Britannica & Gregerson, E. Brownian motion | physics | Britannica. *Encyclopedia Britannica* (2017). Available at: https://www.britannica.com/science/Brownian-motion. (Accessed: 4th August 2021)
37. Feynman, R. *The Feynman Lectures on Physics Vol. I Ch. 41: The Brownian Movement*. *The Feynman Lectures on Physics* (1963).
38. Brunberg, J. A. *et al.* In vivo MR determination of water diffusion coefficients and diffusion anisotropy: Correlation with structural alteration in gliomas of the cerebral hemispheres. *Am. J. Neuroradiol.* **16**, 361–371 (1995).
39. Provenzale, J. M., Mukundan, S. & Barboriak, D. P. Diffusion-weighted and perfusion MR imaging for brain tumor characterization and assessment of treatment response. *Radiology* **239**, 632–649 (2006).
40. Beaulieu, C. The basis of anisotropic water diffusion in the nervous system - A technical review. *NMR in Biomedicine* **15**, 435–455 (2002).
41. Moseley, M. E. *et al.* Diffusion-weighted MR imaging of anisotropic water diffusion in cat central nervous system. *Radiology* **176**, 439–445 (1990).
42. Guo, A. C., Cummings, T. J., Dash, R. C. & Provenzale, J. M. Lymphomas and high-grade astrocytomas: Comparison of water diffusibility and histologic characteristics. *Radiology* **224**, 177–183 (2002).
43. Krabbe, K. *et al.* MR diffusion imaging of human intracranial tumours. *Neuroradiology* **39**, 483–489 (1997).
44. Calli, C. *et al.* Perfusion and diffusion MR imaging in enhancing malignant cerebral tumors. *Eur. J. Radiol.* **58**, 394–403 (2006).
45. Toh, C. H. *et al.* Glioblastoma multiforme with diffusion-weighted magnetic resonance imaging characteristics mimicking primary brain lymphoma: Case report. *J. Neurosurg.* **105**, 132–135 (2006).
46. Okamoto, K., Ito, J., Ishikawa, K., Sakai, K. & Tokiguchi, S. Diffusion-weighted echo-planar MR imaging in differential diagnosis of brain tumors and tumor-like conditions. *Eur. Radiol.* **10**, 1342–1350 (2000).
47. Assaf, Y. & Pasternak, O. Diffusion tensor imaging (DTI)-based white matter mapping in brain research: A review. *Journal of Molecular Neuroscience* **34**, 51–61 (2008).
48. Inoue, T., Ogasawara, K., Beppu, T., Ogawa, A. & Kabasawa, H. Diffusion tensor imaging for preoperative evaluation of tumor grade in gliomas. *Clin. Neurol. Neurosurg.* **107**, 174–180 (2005).

49. Field, A. S., Wu, Y. C. & Alexander, A. L. Principal diffusion direction in peritumoral fiber tracts: Color map patterns and directional statistics. in *Annals of the New York Academy of Sciences* **1064**, 193–201 (Ann N Y Acad Sci, 2005).
50. Goebell, E. *et al.* Disarrangement of fiber tracts and decline of neuronal density correlate in glioma patients - A combined diffusion tensor imaging and1H-MR spectroscopy study. *Am. J. Neuroradiol.* **27**, 1426–1431 (2006).
51. Stieltjes, B. *et al.* Diffusion tensor imaging in primary brain tumors: Reproducible quantitative analysis of corpus callosum infiltration and contralateral involvement using a probabilistic mixture model. *Neuroimage* **31**, 531–542 (2006).
52. Lu, S. *et al.* Diffusion-tensor MR imaging of intracranial neoplasia and associated peritumoral edema: Introduction of the tumor infiltration index. *Radiology* **232**, 221–228 (2004).
53. Van Westen, D., Lätt, J., Englund, E., Brockstedt, S. & Larsson, E. M. Tumor extension in high-grade gliomas assessed with diffusion magnetic resonance imaging: Values and lesion-to-brain ratios of apparent diffusion coefficient and fractional anisotropy. *Acta radiol.* **47**, 311–319 (2006).
54. Sundgren, P. C. *et al.* Differentiation of recurrent brain tumor versus radiation injury using diffusion tensor imaging in patients with new contrast-enhancing lesions. *Magn. Reson. Imaging* **24**, 1131–1142 (2006).
55. Castillo, M., Smith, J. K., Kwock, L. & Wilber, K. Apparent diffusion coefficients in the evaluation of high-grade cerebral gliomas. *Am. J. Neuroradiol.* **22**, 60–64 (2001).
56. Provenzale, J. M., McGraw, P., Mhatre, P., Guo, A. C. & Delong, D. Peritumoral brain regions in gliomas and meningiomas: Investigation with isotropic diffusion-weighted MR imaging and diffusion-tensor MR imaging. *Radiology* **232**, 451–460 (2004).
57. Price, S. J. *et al.* Diffusion tensor imaging of brain tumours at 3 T: A potential tool for assessing white matter tract invasion? *Clin. Radiol.* **58**, 455–462 (2003).
58. Chiang, I. C. *et al.* Distinction between high-grade gliomas and solitary metastases using peritumoral 3-T magnetic resonance spectroscopy, diffusion, and perfusion imagings. *Neuroradiology* **46**, 619–627 (2004).
59. Kono, K. *et al.* The role of diffusion-weighted imaging in patients with brain tumors. *Am. J. Neuroradiol.* **22**, 1081–1088 (2001).
60. Stadnik, T. W. *et al.* Diffusion-weighted MR imaging of intracerebral masses: Comparison with conventional MR imaging and histologic findings. *Am. J. Neuroradiol.* **22**, 969–976 (2001).
61. Lu, S., Ahn, D., Johnson, G. & Cha, S. Peritumoral diffusion tensor imaging of high-grade gliomas and metastatic brain tumors. *Am. J. Neuroradiol.* **24**, 937–941 (2003).
62. Cady, E. B. *et al.* Non-invasive investigation of cerebral metabolism in newborn infants by Phosphorus nuclear magnetic resonance spectroscopy. *Lancet* **321**, 1059–1062 (1983).
63. Zhu, H. & Barker, P. B. MR spectroscopy and spectroscopic imaging of the brain. *Methods in Molecular Biology* **711**, 203–226 (2010).

64. Bottomley, P. A., Edelstein, W. A., Foster, T. H. & Adams, W. A. In vivo solvent-suppressed localized hydrogen nuclear magnetic resonance spectroscopy: A window to metabolism? *Proc. Natl. Acad. Sci. U. S. A.* **82**, 2148–2152 (1985).

65. Gill, S. S. *et al.* Brain metabolites as 1H NMR markers of neuronal and glial disorders. *NMR Biomed.* **2**, 196–200 (1989).

66. Davie, C. A. *et al.* Detection of myelin breakdown products by proton magnetic resonance spectroscopy. *The Lancet* **341**, 630–631 (1993).

67. Brenner, R. E. *et al.* The proton NMR spectrum in acute EAE: The significance of the change in the Cho:Cr ratio. *Magn. Reson. Med.* **29**, 737–745 (1993).

68. Penrice, J. *et al.* Proton magnetic resonance spectroscopy of the brain in normal preterm and term infants, and early changes after perinatal hypoxia-ischemia. *Pediatr. Res.* **40**, 6–14 (1996).

69. Barker, P. B. *et al.* Acute stroke: Evaluation with serial proton MR spectroscopic imaging. *Radiology* **192**, 723–732 (1994).

70. Petroff, O. A. C. *et al.* Spectroscopic imaging of stroke in humans: Histopathology correlates of spectral changes. *Neurology* **42**, 1349–1354 (1992).

71. Alger, J. R. *et al.* Metabolism of human gliomas: Assessment with H-1 MR spectroscopy and F-18 fluorodeoxyglucose PET. *Radiology* **177**, 633–641 (1990).

72. Sijens, P. E., Levendag, P. C., Vecht, C. J., Van Dijk, P. & Oudkerk, M. 1H MR spectroscopy detection of lipids and lactate in metastatic brain tumors. *NMR Biomed.* **9**, 65–71 (1996).

73. Simonsen, C. Z. *et al.* CBF and CBV measurements by USPIO bolus tracking: reproducibility and comparison with Gd-based values. **9**, 342–7 (1999).

74. Østergaard, L. *et al.* Cerebral blood flow measurements by magnetic resonance imaging bolus tracking: Comparison with [15O]H2O positron emission tomography in humans. *Journal of Cerebral Blood Flow and Metabolism* **18**, 935–940 (1998).

75. Østergaard, L., Weisskoff, R. M., Chesler, D. A., Gyldensted, G. & Rosen, B. R. High resolution measurement of cerebral blood flow using intravascular tracer bolus passages. Part I: Mathematical approach and statistical analysis. *Magn. Reson. Med.* **36**, 715–725 (1996).

76. Bolwin, K., Boutchko, R., Budinger, T., Buther, F. & Cunningham, V. *Comprehensive Biomedical Physics, Nuclear Medicine and Molecular Imaging*. (2014).

77. Meier, P. & Zierler, K. L. On the theory of the indicator-dilution method for measurement of blood flow and volume. *J. Appl. Physiol.* **6**, 731–744 (1954).

78. Larsson, H. B. W., Hansen, A. E., Berg, H. K., Rostrup, E. & Haraldseth, O. Dynamic contrast-enhanced quantitative perfusion measurement of the brain using T1-weighted MRI at 3T. *J. Magn. Reson. Imaging* **27**, 754–762 (2008).

79. Taylor, J. S. *et al.* MR imaging of tumor microcirculation: Promise for the new millenium. *J. Magn. Reson. Imaging* **10**, 903–907 (1999).

80. Folkman, J. Role of angiogenesis in tumor growth and metastasis. *Seminars in oncology* **29**, 15–18 (2002).

81. Aronen, H. J. *et al.* Echo-Planar MR Cerebral Blood Volume Mapping of Gliomas: Clinical Utility. *Acta radiol.* **36**, 520–528 (1995).
82. Forsén, S. & Huffman, R. A. Study of moderately rapid chemical exchange reactions by means of nuclear magnetic double resonance. *J. Chem. Phys.* **39**, 2892–2901 (1963).
83. Ward, K. M., Aletras, A. H. & Balaban, R. S. A New Class of Contrast Agents for MRI Based on Proton Chemical Exchange Dependent Saturation Transfer (CEST). *J. Magn. Reson.* **143**, 79–87 (2000).
84. Zhou, J. & Zijl, P. C. M. va. Chemical exchange saturation transfer imaging and spectroscopy. *Progress in Nuclear Magnetic Resonance Spectroscopy* **48**, 109–136 (2006).
85. Sherry, A. D. & Woods, M. Chemical exchange saturation transfer contrast agents for magnetic resonance imaging. *Annual Review of Biomedical Engineering* **10**, 391–411 (2008).
86. Kogan, F., Hariharan, H. & Reddy, R. Chemical Exchange Saturation Transfer (CEST) Imaging: Description of Technique and Potential Clinical Applications. *Curr. Radiol. Rep.* **1**, 102–114 (2013).
87. Vinogradov, E., Sherry, A. D. & Lenkinski, R. E. CEST: From basic principles to applications, challenges and opportunities. *J. Magn. Reson.* **229**, 155–172 (2013).
88. van Zijl, P. C. M., Lam, W. W., Xu, J., Knutsson, L. & Stanisz, G. J. Magnetization Transfer Contrast and Chemical Exchange Saturation Transfer MRI. Features and analysis of the field-dependent saturation spectrum. *Neuroimage* **168**, 222–241 (2018).
89. Zhou, J., Payen, J. F., Wilson, D. A., Traystman, R. J. & Van Zijl, P. C. M. Using the amide proton signals of intracellular proteins and peptides to detect pH effects in MRI. *Nat. Med.* **9**, 1085–1090 (2003).
90. Van Zijl, P. C. M. *et al.* Mechanism of magnetization transfer during on-resonance water saturation. A new approach to detect mobile proteins, peptides, and lipids. *Magn. Reson. Med.* **49**, 440–449 (2003).
91. Zhou, J. *et al.* Practical data acquisition method for human brain tumor amide proton transfer (APT) imaging. *Magn. Reson. Med.* **60**, 842–849 (2008).
92. Brindle, K. M., Izquierdo-García, J. L., Lewis, D. Y., Mair, R. J. & Wright, A. J. Brain tumor imaging. *Journal of Clinical Oncology* **35**, 2432–2438 (2017).
93. Hobbs, S. K. *et al.* Magnetic Resonance Image-Guided Proteomics of Human Glioblastoma Multiforme. *J. Magn. Reson. Imaging* **18**, 530–536 (2003).
94. Yan, K. *et al.* Assessing Amide Proton Transfer (APT) MRI Contrast Origins in 9 L Gliosarcoma in the Rat Brain Using Proteomic Analysis. *Mol. Imaging Biol.* **17**, 479–487 (2015).
95. Howe, F. A. *et al.* Metabolic profiles of human brain tumors using quantitative in vivo 1H magnetic resonance spectroscopy. *Magn. Reson. Med.* **49**, 223–232 (2003).
96. Jiang, S. *et al.* Predicting IDH mutation status in grade II gliomas using amide proton transfer-weighted (APTw) MRI. *Magn. Reson. Med.* **78**, 1100–1109 (2017).

97. Jiang, S. *et al.* Discriminating MGMT promoter methylation status in patients with glioblastoma employing amide proton transfer-weighted MRI metrics. *Eur. Radiol.* **28**, 2115–2123 (2018).
98. Martino, F., Amici, G., Rosner, M., Ronco, C. & Novara, G. Gadolinium-Based Contrast Media Nephrotoxicity in Kidney Impairment: The Physio-Pathological Conditions for the Perfect Murder. *J. Clin. Med.* **10**, 271 (2021).
99. Lum, M. & Tsiouris, A. J. MRI safety considerations during pregnancy. *Clinical Imaging* **62**, 69–75 (2020).
100. Huang, X. X. *et al.* Ischemic Stroke Increased Gadolinium Deposition in the Brain and Aggravated Astrocyte Injury After Gadolinium-Based Contrast Agent Administration: Linear Versus Macrocyclic Agents. *J. Magn. Reson. Imaging* **53**, 1282–1292 (2021).
101. Strickler, S. E. & Clark, K. R. Gadolinium Deposition: A Study Review. *Radiol. Technol.* **92**, 249–258 (2021).
102. Chen, R. *et al.* Parallel Comparative Studies on Mouse Toxicity of Oxide Nanoparticle- and Gadolinium-Based T1 MRI Contrast Agents. *ACS Nano* **9**, 12425–12435 (2015).
103. Ray, D. E., Cavanagh, J. B., Nolan, C. C. & Williams, S. C. R. Neurotoxic effects of gadopentetate dimeglumine: Behavioral disturbance and morphology after intracerebroventricular injection in rats. *Am. J. Neuroradiol.* **17**, 365–373 (1996).
104. Rogosnitzky, M. & Branch, S. Gadolinium-based contrast agent toxicity: a review of known and proposed mechanisms. *BioMetals* **29**, 365–376 (2016).
105. Louis, D. N. *et al.* The 2007 WHO classification of tumours of the central nervous system. *Acta Neuropathologica* **114**, 97–109 (2007).
106. Li, X. *et al.* Discrimination between glioblastoma and solitary brain metastasis: Comparison of inflow-based vascular-space-occupancy and dynamic susceptibility contrast MR imaging. *Am. J. Neuroradiol.* **41**, 583–590 (2020).
107. Hollingworth, W. *et al.* A systematic literature review of magnetic resonance spectroscopy for the characterization of brain tumors. *American Journal of Neuroradiology* **27**, 1404–1411 (2006).
108. Suh, C. H., Kim, H. S., Jung, S. C., Choi, C. G. & Kim, S. J. Perfusion MRI as a diagnostic biomarker for differentiating glioma from brain metastasis: a systematic review and meta-analysis. *European Radiology* **28**, 3819–3831 (2018).
109. Usinskiene, J. *et al.* Optimal differentiation of high- and low-grade glioma and metastasis: a meta-analysis of perfusion, diffusion, and spectroscopy metrics. *Neuroradiology* **58**, 339–350 (2016).
110. Suh, C. H. *et al.* Amide proton transfer-weighted MRI in distinguishing high- and low-grade gliomas: a systematic review and meta-analysis. *Neuroradiology* **61**, 525–534 (2019).
111. Okuchi, S. *et al.* Diagnostic accuracy of dynamic contrast-enhanced perfusion MRI in stratifying gliomas: A systematic review and meta-analysis. *Cancer Med.* **8**, 5564–5573 (2019).

112. Fouke, S. J. *et al.* The role of imaging in the management of adults with diffuse low grade glioma: A systematic review and evidence-based clinical practice guideline. *Journal of Neuro-Oncology* **125**, 457–479 (2015).

113. van Lent, D. I., van Baarsen, K. M., Snijders, T. J. & Robe, P. A. J. T. Radiological differences between subtypes of WHO 2016 grade II–III gliomas: a systematic review and meta-analysis. *Neuro-Oncology Adv.* **2**, (2020).

114. Tabatabaei, M. *et al.* Current Status and Quality of Machine Learning-Based Radiomics Studies for Glioma Grading: A Systematic Review. *Oncology* **99**, 433–443 (2021).

115. Jian, A. *et al.* Machine Learning for the Prediction of Molecular Markers in Glioma on Magnetic Resonance Imaging: A Systematic Review and Meta-Analysis. *Neurosurgery* **89**, 31–44 (2021).

116. Hosmer, D. W., Lemeshow, S. & Sturdivant, R. X. *Applied Logistic Regression: Third Edition*. *Applied Logistic Regression: Third Edition* (wiley, 2013). doi:10.1002/9781118548387

117. Harrell, F. E., Lee, K. L. & Mark, D. B. Prognostic/Clinical Prediction Models: Multivariable Prognostic Models: Issues in Developing Models, Evaluating Assumptions and Adequacy, and Measuring and Reducing Errors. *Tutorials Biostat. Stat. Methods Clin. Stud.* **1**, 223–249 (2005).

118. Ranganathan, P., Pramesh, C. & Aggarwal, R. Common pitfalls in statistical analysis: Logistic regression. *Perspect. Clin. Res.* **8**, 148–151 (2017).

119. Vittinghoff, E. & McCulloch, C. E. Relaxing the rule of ten events per variable in logistic and cox regression. *Am. J. Epidemiol.* **165**, 710–718 (2007).

120. Alfonso, J. C. L. *et al.* The biology and mathematical modelling of glioma invasion: A review. *Journal of the Royal Society Interface* **14**, (2017).

121. Suh, C. H. *et al.* MRI as a diagnostic biomarker for differentiating primary central nervous system lymphoma from glioblastoma: A systematic review and meta-analysis. *J. Magn. Reson. Imaging* **50**, 560–572 (2019).

122. Hourani, R. *et al.* Can proton MR spectroscopic and perfusion imaging differentiate between neoplastic and nonneoplastic brain lesions in adults? *Am. J. Neuroradiol.* **29**, 366–372 (2008).

123. Server, A. *et al.* Proton magnetic resonance spectroscopy in the distinction of high-grade cerebral gliomas from single metastatic brain tumors. *Acta radiol.* **51**, 316–325 (2010).

124. Wang, Q. *et al.* The diagnostic performance of magnetic resonance spectroscopy in differentiating high-from low-grade gliomas: A systematic review and meta-analysis. *Eur. Radiol.* **26**, 2670–2684 (2016).

125. Sotirios, B., Demetriou, E., Topriceanu, C. C. & Zakrzewska, Z. The role of APT imaging in gliomas grading: A systematic review and meta-analysis. *Eur. J. Radiol.* **133**, 109353 (2020).

126. Strugar, J., Rothbart, D., Harrington, W. & Criscuolo, G. R. Vascular permeability factor in brain metastases: Correlation with vasogenic brain edema and tumor angiogenesis. *J. Neurosurg.* **81**, 560–566 (1994).

127. Helenius, J. *et al.* Diffusion-weighted MR imaging in normal human brains in various age groups. *Am. J. Neuroradiol.* **23**, 194–199 (2002).
128. Jellison, B. J. *et al.* Diffusion Tensor Imaging of Cerebral White Matter: A Pictorial Review of Physics, Fiber Tract Anatomy, and Tumor Imaging Patterns. *American Journal of Neuroradiology* **25**, 356–369 (2004).
129. Lee, E. J. *et al.* Diagnostic value of peritumoral minimum apparent diffusion coefficient for differentiation of glioblastoma multiforme from solitary metastatic lesions. *Am. J. Roentgenol.* **196**, 71–76 (2011).
130. Rollin, N. *et al.* Clinical relevance of diffusion and perfusion magnetic resonance imaging in assessing intra-axial brain tumors. *Neuroradiology* **48**, 150–159 (2006).
131. Law, M. *et al.* Comparison of cerebral blood volume and vascular permeability from dynamic susceptibility contrast-enhanced perfusion MR imaging with glioma grade. *Am. J. Neuroradiol.* **25**, 746–755 (2004).
132. Maia, A. C. M. *et al.* MR cerebral blood volume maps correlated with vascular endothelial growth factor expression and tumor grade in nonenhancing gliomas. *Am. J. Neuroradiol.* **26**, 777–783 (2005).
133. Fan, G. G., Deng, Q. L., Wu, Z. H. & Guo, Q. Y. Usefulness of diffusion/perfusion-weighted MRI in patients with non-enhancing supratentorial brain gliomas: A valuable tool to predict tumour grading? *Br. J. Radiol.* **79**, 652–658 (2006).
134. Yoon, J. H. *et al.* Grading of cerebral glioma with multiparametric MR imaging and 18F-FDG-PET: Concordance and accuracy. *Eur. Radiol.* **24**, 380–389 (2014).
135. McBride, D. Q. *et al.* Analysis of brain tumors using 1H magnetic resonance spectroscopy. *Surg. Neurol.* **44**, 137–144 (1995).
136. Sijens, P. E. & Oudkerk, M. 1H chemical shift imaging characterization of human brain tumor and edema. *Eur. Radiol.* **12**, 2056–2061 (2002).
137. Yang, D. *et al.* Cerebral gliomas: Prospective comparison of multivoxel 2D chemical-shift imaging proton MR spectroscopy, echoplanar perfusion and diffusion-weighted MRI. *Neuroradiology* **44**, 656–666 (2002).
138. Zeng, Q. S., Liu, H. P., Zhang, K., Li, C. F. & Zhou, G. Y. Noninvasive evaluation of cerebral glioma grade by using multivoxel 3D proton MR spectroscopy. *Magn. Reson. Imaging* **29**, 25–31 (2011).
139. Law, M. *et al.* Glioma Grading: Sensitivity, Specificity, and Predictive Values of Perfusion MR Imaging and Proton MR Spectroscopic Imaging Compared with Conventional MR Imaging. *Am. J. Neuroradiol.* **24**, 1989–1998 (2003).
140. Bulakbasi, N., Kocaoglu, M., Örs, F., Tayfun, C. & Ügöz, T. Combination of single-voxel proton MR spectroscopy and apparent diffusion coefficient calculation in the evaluation of common brain tumors. *Am. J. Neuroradiol.* **24**, 225–233 (2003).
141. Costanzo, A. *et al.* Multiparametric 3T MR approach to the assessment of cerebral gliomas: Tumor extent and malignancy. *Neuroradiology* **48**, 622–631 (2006).
142. Zonari, P., Baraldi, P. & Crisi, G. Multimodal MRI in the characterization of glial neoplasms: The combined role of single-voxel MR spectroscopy, diffusion imaging and echo-planar perfusion imaging. *Neuroradiology* **49**, 795–803 (2007).

143. Malach, T. & Pomenkova, J. Comparing classifier's performance based on confidence interval of the ROC. *Radioengineering* **27**, 827–834 (2018).
144. Brown, C. D. & Davis, H. T. Receiver operating characteristics curves and related decision measures: A tutorial. *Chemom. Intell. Lab. Syst.* **80**, 24–38 (2006).
145. Hanley, J. A. & McNeil, B. J. A method of comparing the areas under receiver operating characteristic curves derived from the same cases. *Radiology* **148**, 839–843 (1983).
146. Westin, L. K. *Receiver operating characteristic (ROC) analysis. Evaluating discriminance effects among decision support systems*.
147. Tien Bui, D., Tuan, T. A., Klempe, H., Pradhan, B. & Revhaug, I. Spatial prediction models for shallow landslide hazards: a comparative assessment of the efficacy of support vector machines, artificial neural networks, kernel logistic regression, and logistic model tree. *Landslides* **13**, 361–378 (2016).
148. Yan, H., Bigner, D. D., Velculescu, V. & Parsons, D. W. Mutant metabolic enzymes are at the origin of gliomas. *Cancer Research* **69**, 9157–9159 (2009).
149. Hegi, M. E. *et al.* Clinical Trial Substantiates the Predictive Value of O-6-Methylguanine-DNA Methyltransferase Promoter Methylation in Glioblastoma Patients Treated with Temozolomide. *Clin. Cancer Res.* **10**, 1871–1874 (2004).
150. Drabycz, S. *et al.* An analysis of image texture, tumor location, and MGMT promoter methylation in glioblastoma using magnetic resonance imaging. *Neuroimage* **49**, 1398–1405 (2010).
151. Gupta, A. *et al.* Diffusion-weighted MR imaging and MGMT methylation status in glioblastoma: A reappraisal of the role of preoperative quantitative ADC measurements. *American Journal of Neuroradiology* **34**, E10 (2013).
152. Ahn, S. S. *et al.* Prediction of methylguanine methyltransferase promoter methylation in glioblastoma using dynamic contrast-enhanced magnetic resonance and diffusion tensor imaging: Clinical article. *J. Neurosurg.* **121**, 367–373 (2014).
153. Moon, W. J., Choi, J. W., Roh, H. G., Lim, S. D. & Koh, Y. C. Imaging parameters of high grade gliomas in relation to the MGMT promoter methylation status: The CT, diffusion tensor imaging, and perfusion MR imaging. *Neuroradiology* **54**, 555–563 (2012).
154. Pope, W. B. *et al.* Apparent diffusion coefficient histogram analysis stratifies progression-free survival in newly diagnosed bevacizumab-treated glioblastoma. *Am. J. Neuroradiol.* **32**, 882–889 (2011).
155. Chen, R., Smith-Cohn, M., Cohen, A. L. & Colman, H. Glioma Subclassifications and Their Clinical Significance. *Neurotherapeutics* **14**, 284–297 (2017).
156. Schwartzentruber, J. *et al.* Driver mutations in histone H3.3 and chromatin remodelling genes in paediatric glioblastoma. *Nature* **482**, 226–231 (2012).
157. Perazella, M. Gadolinium-Contrast Toxicity in Patients with Kidney Disease: Nephrotoxicity and Nephrogenic Systemic Fibrosis. *Curr. Drug Saf.* **3**, 67–75 (2008).